

# Axial and Vector Structure Functions for Electron- and Neutrino-Nucleon Scattering Cross Sections at all $Q^2$ using Effective Leading order Parton Distribution Functions

Arie Bodek<sup>a</sup>, and Un-ki Yang<sup>b</sup>

<sup>a</sup>Department of Physics and Astronomy, University of Rochester, Rochester, New York, 14618, USA

<sup>b</sup>School of Physics and Astronomy, the University of Manchester, Manchester, M13 9PL, U.K.

We construct a model for inelastic neutrino- and electron-nucleon scattering cross sections using effective leading order parton distribution functions with a new scaling variable  $\xi_w$ . Non-perturbative effects are well described using the  $\xi_w$  scaling variable, in combination with multiplicative  $K$  factors at low  $Q^2$ . Our model describes all inelastic charged lepton-nucleon scattering (including resonance) data (HERA/NMC/BCDMS/SLAC/JLab) ranging from very high  $Q^2$  to very low  $Q^2$  and down to the photo-production region. The model describes existing inelastic neutrino-nucleon scattering measurements, and has been developed to be used in analysis of neutrino oscillation experiments in the few GeV region.

## 1. Introduction

The field of neutrino oscillation physics has progressed from the discovery of neutrino oscillation [1] to an era of precision measurements of mass splitting and mixing angles. The cross sections for neutrino interactions in the few GeV region are not well known. This results in large systematic uncertainties in the extraction of mass splitting and mixing parameters in neutrino oscillations experiments such as MINOS[2], NO $\nu$ A[3], K2K [4], SuperK[6], T2K[5], and MiniBooNE[7]. A reliable model of neutrino inelastic cross sections at low energies is essential for precise neutrino oscillations experiments.

The renewed interest in neutrino interactions at low energies has resulted in the construction of several near detectors (e.g. MINOS[2], T2K[5]) to measure low energy cross sections and fluxes. In addition, there are new experiments (e.g. SciBooNE [8], and MINERvA[9]) which are specifically designed to measure neutrino cross sections at low energies.

In this communication, we report on a duality based model of neutrino interactions. Earlier versions of the model[10,11] have been incorporated into several Monte Carlo genera-

tors of neutrino interactions including NEUT[12], GENIE[13], NEUGEN[14] and NUANCE[15].

In the few GeV region, the three types of neutrino interaction processes include quasi-elastic reactions, resonance production, and deep inelastic scattering. It is quite challenging to disentangle each of those contributions separately, and in particular the contribution of resonance production and inelastic scattering continuum. At low  $Q^2$  there are large non-perturbative contributions to the inelastic cross section. These include kinematic target mass corrections, dynamic higher twist effects, and higher order Quantum Chromodynamic (QCD) terms.

In our previous studies [16,17,18], non-perturbative effects were investigated within Leading Order (LO), Next-to-Leading Order (NLO) and Next-to-Next Leading Order (NNLO) QCD using charged lepton-nucleon scattering experimental data [19,20,21]. We found that in NLO QCD, most of the empirical higher-twist terms needed to obtain good agreement with the low energy data for  $Q^2 > 1$  (GeV/c)<sup>2</sup> originate primarily from target mass effects and the missing NNLO terms (i.e. not from interactions with spectator quarks). If such is the case, then

these terms should be the same in charged leptons ( $e$ ,  $\mu$ ) and neutrino ( $\nu_\mu$ ) scattering. Therefore, low energy  $\nu_\mu$  data can be described by effective Parton Distribution Functions (PDFs) which are fit to high  $Q^2$  charged lepton-nucleon scattering data, but modified to include target mass and higher-twist corrections that are extracted from low energy  $e/\mu$  scattering data. For  $Q^2 < 1$  (GeV/c)<sup>2</sup> additional corrections for non-perturbative effects from spectator quarks are required. These corrections can be parametrized as multiplicative  $K$  factors. For the vector part of the charged current interaction the  $K$  factor terms should be the same in  $\nu_\mu$  and  $e/\mu$  scattering.

Therefore, a model that describes electron and muon scattering can also be used to model neutrino scattering. At high  $Q^2$  the vector and axial structure functions are expected to be the same. The only terms which are not constrained by muon and electron scattering are terms which describe the difference between axial and vector structure functions and form factors at low values of  $Q^2$ .

## 2. Electron-nucleon and muon-nucleon scattering

In this section we define the kinematic variables for the case of charged lepton scattering from neutrons and protons. The differential cross section for scattering of an unpolarized charged lepton with an incident energy  $E_0$ , final energy  $E'$  and scattering angle  $\theta$  can be written in terms of the structure functions  $\mathcal{F}_1$  and  $\mathcal{F}_2$  as:

$$\frac{d^2\sigma}{d\Omega dE'}(E_0, E', \theta) = \frac{4\alpha^2 E'^2}{Q^4} \cos^2(\theta/2) \times [\mathcal{F}_2(x, Q^2)/\nu + 2 \tan^2(\theta/2) \mathcal{F}_1(x, Q^2)/M]$$

where  $\alpha$  is the fine structure constant,  $M$  is the nucleon mass,  $\nu = E_0 - E'$  is energy of the virtual photon which mediates the interaction,  $Q^2 = 4E_0 E' \sin^2(\theta/2)$  is the invariant four-momentum transfer squared, and  $x = Q^2/2M\nu$  is a measure of the longitudinal momentum carried by the struck partons.

Alternatively, one could view this scattering process as virtual photon absorption. Unlike the

real photon, the virtual photon can have two modes of polarization. In terms of the cross section for the absorption of transverse ( $\sigma_T$ ) and longitudinal ( $\sigma_L$ ) virtual photons, the differential cross section can be written as,

$$\frac{d^2\sigma}{d\Omega dE'} = \Gamma [\sigma_T(x, Q^2) + \epsilon \sigma_L(x, Q^2)] \quad (1)$$

where,

$$\Gamma = \frac{\alpha K E'}{4\pi^2 Q^2 E_0} \left( \frac{2}{1 - \epsilon} \right) \quad (2)$$

$$\epsilon = \left[ 1 + 2 \left( 1 + \frac{Q^2}{4M^2 x^2} \right) \tan^2 \frac{\theta}{2} \right]^{-1} \quad (3)$$

$$K = \frac{2M\nu - Q^2}{2M}. \quad (4)$$

The quantities  $\Gamma$  and  $\epsilon$  represent the flux and the degree of longitudinal polarization of the virtual photons respectively. The quantity  $R$ , is defined as the ratio  $\sigma_L/\sigma_T$ , and is related to the structure functions by,

$$R(x, Q^2) = \frac{\sigma_L}{\sigma_T} = \frac{\mathcal{F}_2}{2x\mathcal{F}_1} \left( 1 + \frac{4M^2 x^2}{Q^2} \right) - 1 = \frac{\mathcal{F}_L}{2x\mathcal{F}_1} \quad (5)$$

where  $\mathcal{F}_L$  is called the longitudinal structure function. The structure functions are expressed in terms of  $\sigma_L$  and  $\sigma_T$  as follows:

$$\mathcal{F}_1 = \frac{MK}{4\pi^2 \alpha} \sigma_T, \quad (6)$$

$$\mathcal{F}_2 = \frac{\nu K (\sigma_L + \sigma_T)}{4\pi^2 \alpha \left( 1 + \frac{Q^2}{4M^2 x^2} \right)} \quad (7)$$

$$\mathcal{F}_L(x, Q^2) = \mathcal{F}_2 \left( 1 + \frac{4M^2 x^2}{Q^2} \right) - 2x\mathcal{F}_1 \quad (8)$$

or,

$$2x\mathcal{F}_1 = \mathcal{F}_2 \left( 1 + \frac{4M^2 x^2}{Q^2} \right) - \mathcal{F}_L(x, Q^2). \quad (9)$$

Standard PDFs are extracted from global fits to various sets of deep inelastic (DIS) scattering data at high energies and high  $Q^2$ , where non-perturbative QCD effects are negligible. PDF fits are performed within the framework of QCD in

either LO, NLO or NNLO. Here, using a new scaling variable ( $\xi_w$ ) we construct effective LO PDFs that account for the contributions from target mass corrections, non-perturbative QCD effects, and higher order QCD terms.

### 3. The basic model: First iteration with GRV98 PDFs .

Our proposed scaling variable,  $\xi_w$  is derived as follows. Using energy momentum conservation, the factional momentum,  $\xi$  carried by a quark in a proton target of mass  $M$  is

$$\xi = \frac{2xQ'^2}{Q^2(1 + \sqrt{1 + 4M^2x^2/Q^2})}, \quad (10)$$

where

$$2Q'^2 = [Q^2 + M_f^2 - M_i^2] + \sqrt{(Q^2 + M_f^2 - M_i^2)^2 + 4Q^2(M_i^2 + P_T^2)}$$

Here  $M_i$  is the initial quark mass with average initial transverse momentum  $P_T$ , and  $M_f$  is the mass of the final state quark. This expression for  $\xi$  was previously derived [22] for the case of  $P_T = 0$ .

Assuming  $M_i = 0$  we construct following scaling variable

$$\xi_w = \frac{2x(Q^2 + M_f^2 + B)}{Q^2[1 + \sqrt{1 + 4M^2x^2/Q^2}] + 2Ax}, \quad (11)$$

or alternatively

$$\xi_w = \frac{(Q^2 + M_f^2 + B)}{M\nu[1 + \sqrt{1 + Q^2/\nu^2}] + A}, \quad (12)$$

where in general  $M_f = 0$ , except for the case of charm-production in neutrino scattering for which  $M_f = 1.32 \text{ (GeV/c)}^2$ . The parameter  $A$  is used to account (on average) for the higher order QCD terms and dynamic higher twist in the form of an enhanced target mass term (the effects of the proton target mass is already taken into account in the denominator of  $\xi_w$ ). The parameter  $B$  is used to account (on average) for the initial state quark transverse momentum, and also for the effective mass of the final state quark originating from multi-gluon emission. A non-zero  $B$

also allows us to describe data in the photoproduction limit (all the way down to  $Q^2=0$ ).

In leading order QCD (e.g. GRV98 PDFs),  $\mathcal{F}_{2,LO}$  for the scattering of electrons and muons on proton (or neutron) targets is given by the sum of quark and anti-quark distributions (each weighted the square of the quark charges):

$$\mathcal{F}_{2,LO}^{e/\mu}(x, Q^2) = \sum_i e_i^2 [xq_i(x, Q^2) + x\bar{q}_i(x, Q^2)]. \quad (13)$$

Our proposed effective LO PDFs model includes the following:

1. The GRV98 LO Parton Distribution Functions (PDFs) [23] are used to describe  $\mathcal{F}_{2,LO}^{e/\mu}(x, Q^2)$ . The minimum  $Q^2$  value for these PDFs is  $0.8 \text{ (GeV/c)}^2$ .
2. The scaling variable  $x$  is replaced with the scaling variable  $\xi_w$  as defined in Eq. 11. Here,

$$\mathcal{F}_{2,LO}^{e/\mu}(x, Q^2) = \sum_i e_i^2 \times [\xi_w q_i(\xi_w, Q^2) + \xi_w \bar{q}_i(\xi_w, Q^2)]. \quad (14)$$

3. As done in earlier non-QCD based fits [24, 26, 27] to low energy charged lepton scattering data, we multiply all PDFs by vector  $K$  factors such that they have the correct form in the low  $Q^2$  photo-production limit. Here we use different forms for the sea and valence quarks. separately;

$$\begin{aligned} K_{sea}^{vector}(Q^2) &= \frac{Q^2}{Q^2 + C_s} \\ K_{valence}^{vector}(Q^2) &= [1 - G_D^2(Q^2)] \\ &\times \left( \frac{Q^2 + C_{v2}}{Q^2 + C_{v1}} \right) \end{aligned} \quad (15)$$

where  $G_D = 1/(1 + Q^2/0.71)^2$  is the proton elastic form factor. This form for the  $K$  factor for valence quarks is motivated by the closure arguments [28] and the Adler [29, 30] sum rule. At low  $Q^2$ ,  $[1 - G_D^2(Q^2)]$  is approximately  $Q^2/(Q^2 + 0.178)$ . which is close to our earlier fit result [10].

These modifications are included in order to describe low  $Q^2$  data in the photoproduction limit ( $Q^2=0$ ), where  $\mathcal{F}_2^{e/\mu}(x, Q^2)$  is related to the photoproduction cross section according to

$$\begin{aligned}\sigma(\gamma p) &= \frac{4\pi^2\alpha}{Q^2} \mathcal{F}_2^{e/\mu}(x, Q^2) \\ &= \frac{0.112 \text{ mb}}{Q^2} \mathcal{F}_2^{e/\mu}(x, Q^2)\end{aligned}\quad (16)$$

4. We freeze the evolution of the GRV98 PDFs at a value of  $Q^2 = 0.80 \text{ (GeV/c)}^2$ . Below this  $Q^2$ ,  $\mathcal{F}_2$  is given by;

$$\begin{aligned}\mathcal{F}_2^{e/\mu}(x, Q^2 < 0.8) &= \\ K_{valence}^{vector}(Q^2) \mathcal{F}_{2,LO}^{valence}(\xi_w, Q^2 = 0.8) \\ + K_{sea}^{vector}(Q^2) \mathcal{F}_{2,LO}^{sea}(\xi_w, Q^2 = 0.8)\end{aligned}\quad (17)$$

5. Finally, we fit for the parameters of the modified effective GRV98 LO PDFs (e.g.  $\xi_w$ ) to inelastic charged lepton scattering data on hydrogen and deuterium targets (SLAC[19]/BCDMS[20]/NMC[21]/H1[31]. In this first iteration, only data with an invariant final state mass  $W > 2 \text{ GeV}/c^2$  are included, where  $W^2 = M^2 + 2M\nu - Q^2$ .

We obtain an excellent fit with the following initial parameters:  $A=0.419$ ,  $B=0.223$ , and  $C_{v1}=0.544$ ,  $C_{v2}=0.431$ , and  $C_{sea}=0.380$ , with  $\chi^2/DOF = 1235/1200$ . Because of these additional  $K$  factors, we find that the GRV98 PDFs need to be scaled up by a normalization factor  $N=1.011$ . Here the parameters are in units of  $(\text{GeV}/c)^2$ . These parameters are summerised in Table 1.

Thus, in our first iteration we modify the GRV98  $\mathcal{F}_2$  to describe low energy data down to photo-production limit as follows:

$$\begin{aligned}\mathcal{F}_2^{e/\mu}(x, Q^2) &= \frac{Q^2}{Q^2 + 0.380} \mathcal{F}_{2,LO}^{sea}(\xi_w, Q^2) \\ &+ (1 - G_D^2) \frac{Q^2 + 0.431}{Q^2 + 0.544} \mathcal{F}_{2,LO}^{valence}(\xi_w, Q^2),\end{aligned}\quad (18)$$

$$\text{where } \xi_w = \frac{2x(Q^2 + 0.223)}{Q^2[1 + \sqrt{1 + (2Mx)^2/Q^2}] + 2*0.419x}.$$

$A$	$B$	$C_{v1}$	$C_{v2}$	$\chi^2/ndf$
0.419	0.223	0.554	0.31	1235/1200
$C_{sea}$			$N$	$\mathcal{F}_{valence}$
0.380			1.011	$[1 - G_D^2(Q^2)]$

Table 1

First Iteration with GRV98 PDFs: Vector Parameters. Only inelastic electron and muon scattering on hydrogen and deuterium (in the continuum region  $W > 2 \text{ GeV}/c^2$ ) are used in the fit. Here the parameters are in units of  $(\text{GeV}/c)^2$ .

In fitting for the effective LO PDFs, the structure functions data are corrected for the relative normalizations between the SLAC, BCDMS, NMC and H1 data (which are allowed to float within the quoted normalization errors). A systematic error shift is applied to the BCDMS data to account for the uncertainty in their magnetic field, as described in the BCDMS publication[20]. All deuterium data are corrected with a small correction for nuclear binding effects [16,17,18] as described in section 12. We also include a separate additional charm production contribution using the photon-gluon fusion model in order to fit the very high energy HERA data. This contribution is not necessary for any of the low energy comparisons, but is necessary to describe the very high energy low  $Q^2$  HERA  $\mathcal{F}_2$  and photoproduction data. The charm contribution must be added separately because the GRV98 PDFs do not include a charm sea. Alternatively, one may use a charm sea parametrization from another PDF.

The first iteration fit successfully describes all inelastic electron and muon scattering data in the continuum region including the very high and very low  $Q^2$  regions. We find that although photo-production data were not included in our first iteration fit, the predictions of our model for the photo-production cross sections on protons and deuterons ( $Q^2 = 0$  limit) are also in good agreement with photoproduction measurements[32].

Furthermore, although no resonance data were included in the first iteration fit, the fit also provides a reasonable description of the average value

of  $\mathcal{F}_2$  for SLAC and Jefferson data in the resonance region [33] (down to  $Q^2 = 0.07 \text{ (GeV/c)}^2$ ).

#### 4. Second iteration with GRV98: Including photo-production data, resonances, and additional parameters

We now describe the second iteration of the fit [11]. Theoretically, the  $K_i$  factors in Eq. 15 are not required to be the same for the  $u$  and  $d$  valence quarks or for the  $u$ ,  $d$ ,  $s$ , sea quarks and antiquarks. In order to allow flexibility in our effective LO model, we treat the  $K_i$  factors for  $u$  and  $d$  valence and for sea quarks and antiquarks separately.

In this second iteration, in order to get additional constraints on the different  $K_i$  factors for up and down quarks separately, we include photo-production data in the continuum region ( $W > 2 \text{ (GeV/c)}^2$ ) for both hydrogen and deuterium. We also include electron scattering data in the resonance region (on hydrogen and deuterium) in the fit. In order to extract neutron cross section from photoproduction cross sections on deuterium, we apply a small shadowing correction as shown in figure 1. The small nuclear binding corrections for the inelastic lepton scattering data on deuterium is described in section 13.

$$\begin{aligned}
K^{LW} &= \frac{\nu^2 + C^{L-Ehad}}{\nu^2} \\
K_{sea-strange}^{vector}(Q^2) &= \frac{Q^2}{Q^2 + C_{sea-strange}^{vector}} \\
K_{sea-up}^{vector}(Q^2) &= \frac{Q^2}{Q^2 + C_{sea-up}^{vector}} \\
K_{sea-down}^{vector}(Q^2) &= \frac{Q^2}{Q^2 + C_{sea-down}^{vector}} \\
K_{valence-up}^{vector}(Q^2) &= K^{LW} [1 - G_D^2(Q^2)] \\
&\quad \times \left( \frac{Q^2 + C_{v2u}^{vector}}{Q^2 + C_{v1u}^{vector}} \right) \\
K_{valence-down}^{vector}(Q^2) &= K^{LW} [1 - G_D^2(Q^2)] \\
&\quad \times \left( \frac{Q^2 + C_{v2d}^{vector}}{Q^2 + C_{v1d}^{vector}} \right) \quad (19)
\end{aligned}$$

The best fit is given by  $A = 0.621 \pm 0.009$ ,  $B = 0.380 \pm 0.004$ ,  $C_{v1d}^{vector} = 0.341 \pm 0.007$ ,  $C_{v1u}^{vector} =$

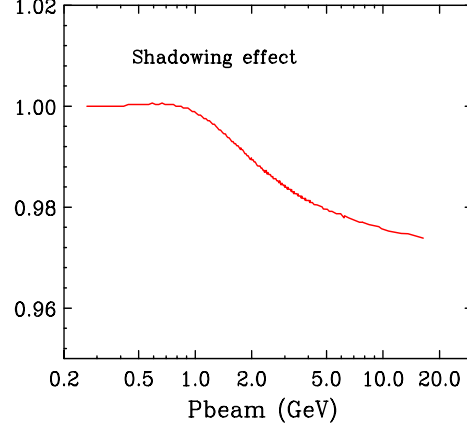


Figure 1. The ratio of photoproduction cross sections on deuterium to the sum of the photoproduction cross sections on unbound protons and neutrons. This shadowing correction is used to extract the photoproduction cross section on free neutrons and protons.

$0.417 \pm 0.024$ ,  $C_{v2d}^{vector} = 0.323 \pm 0.051$ ,  $C_{v2u}^{vector} = 0.264 \pm 0.015$ , and  $C^{L-Ehad} = 0.217 \pm 0.015$ . The sea factors are  $C_{sea-down}^{vector} = 0.621$ ,  $C_{sea-up}^{vector} = 0.363$ , and  $C_{sea-strange}^{vector}$  was set to be the same as  $C_{sea-down}^{vector}$ . Here, the parameters are in units of  $(\text{GeV/c})^2$ . The fit  $\chi^2/\text{DOF} = 2357/1717$ , and  $N = 1.026 \pm 0.003$ . The resonance data add to the  $\chi^2/\text{ndf}$  because the fit only provides a smooth average over the resonances. No neutrino data are included in the fit. These parameters are summarized in Table 2.

The normalization of the various experiments were allowed to float within their errors with the normalization of the SLAC proton data set to 1.0. The fit yields normalization factors of  $0.986 \pm 0.002$ ,  $0.979 \pm 0.003$ ,  $0.998 \pm 0.003$ ,  $1.008 \pm 0.003$ ,  $1.001 \pm 0.004$ , and  $0.987 \pm 0.005$  for the SLAC deuterium data, BCDMS proton data, BCDMS deuterium data, NMC proton data, NMC deuterium data, and H1 proton data, respectively. With these normalization, the GRV PDFs with our modifications should be multiplied by  $N = 1.026 \pm 0.003$ .

$A$	$B$	$C_{v2d}$	$C_{v2u}$
0.621	0.380	0.323	0.264
$C_{sea}^{down}$	$C_{sea}^{up}$	$C_{v1d}$	$C_{v1u}$
0.561	0.369	0.341	0.417
$C_{sea}^{strange}$	$C^{L-Ehad}$	$K_{\nu-d}^{\Delta 1232}$	$K_{\nu-u}^{\Delta 1232}$
0.561	0.218	1.65	0.55
$\chi^2/ndf$	$\mathcal{F}_{valence}$	$N$	
2357/1717	$[1 - G_D^2(Q^2)]$	1.026	

Table 2

Second iteration with GRV98 PDFs: Vector Parameters. Here, we now include electron scattering data in the resonance region and photoproduction data on hydrogen and deuterium. The resonance data adds to the  $\chi^2/ndf$  because the fit provides a smooth average over the resonances. No neutrino data are included in the fit. When applicable, all parameters are in units of  $(GeV/c)^2$ .

Note that we apply also a small  $d/u$  correction to the GRV98 PDFs as described in section 14. This correction increases the  $d$  quark distribution at large  $x$  and is extracted from NMC data for  $\mathcal{F}_2^D/\mathcal{F}_2^P$ .

As seen in the plots, our fit describes all of the data, including photoproduction data in the continuum region. In the resonance region, the fit works well, except near  $Q^2 = 0$ . In order to better describe the resonance region near  $Q^2 = 0$  we include the low  $W$   $K^{LW}$  factor, where  $K^{LW} = (\nu^2 + C^{L-Ehad})/(\nu^2)$ .

For neutrino scattering we must treat the  $I = 3/2$   $\Delta 1232$  resonance as a special case for all values of  $Q^2$ . This is because the neutrino-proton charged current scattering amplitude for the production of the  $\Delta(1232)$   $I = 3/2$  resonance is  $\sqrt{3}$  times the amplitude in neutrino-neutron scattering[34,35]. Similarly, the antineutrino-neutron charged current scattering amplitude for production of the  $\Delta(1232)$   $I = 3/2$  resonance is  $\sqrt{3}$  times the amplitude for the production in neutrino-proton scattering. This relationship holds for both the vector and axial amplitudes.

Therefore, for the case of charged current neutrino and antineutrino scattering the  $K^{LW}$  fac-

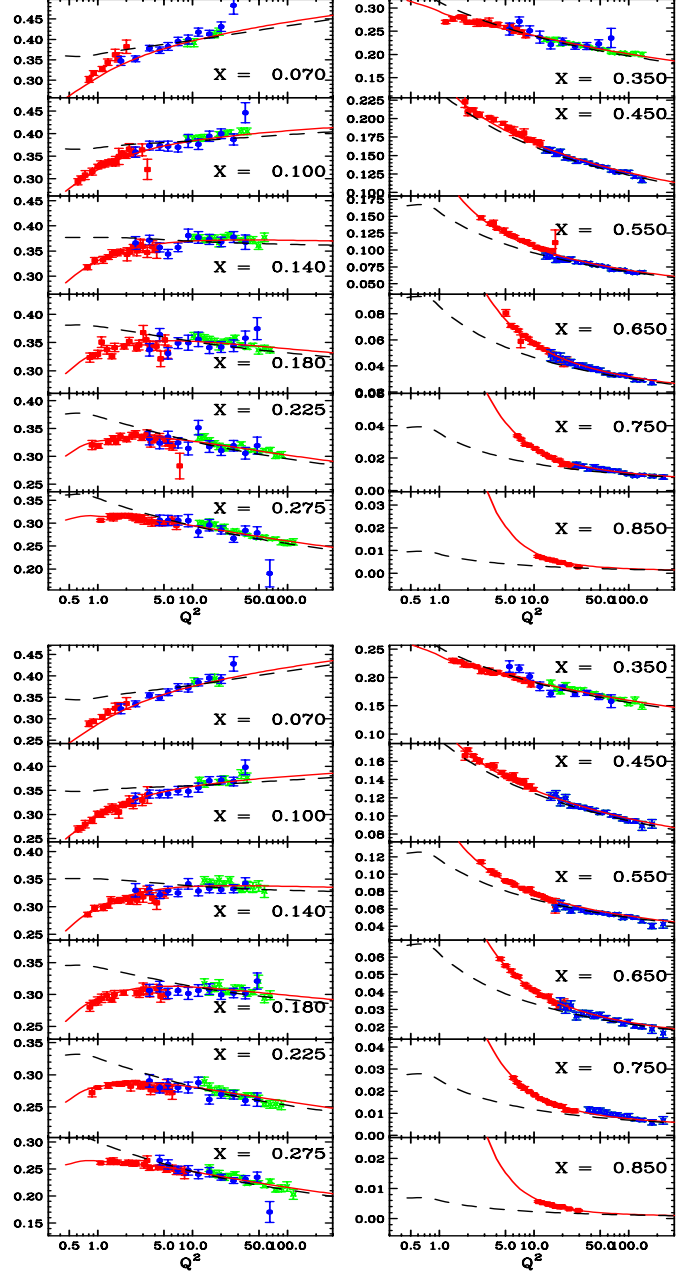


Figure 2. The effective LO PDF model compared to charged lepton  $\mathcal{F}_2$  experimental data (SLAC, BCDMS, NMC) at high  $x$  (these data are included in our fit) :[top]  $\mathcal{F}_2$  proton, [bot]  $\mathcal{F}_2$  deuteron. The solid lines are our fit, and the dashed lines are GRV98 .

tors for the valence  $u$  and  $d$  quark distributions are modified as follows:

$$\begin{aligned}
K_{\nu d}^{LW} &= \frac{\nu^2 + C^{L-Ehad}}{\nu^2} \quad (W > 1.4 \text{ GeV}/c^2) \\
K_{\nu u}^{LW} &= \frac{\nu^2 + C^{L-Ehad}}{\nu^2} \quad (W > 1.4 \text{ GeV}/c^2) \\
K_{\nu d}^{LW} &= K_{\nu d}^{\Delta 1232} = 1.65 \quad (W < 1.4 \text{ GeV}/c^2) \\
K_{\nu u}^{LW} &= K_{\nu u}^{\Delta 1232} = 0.55 \quad (W < 1.4 \text{ GeV}/c^2)
\end{aligned}$$

Comparisons of our fit to various sets of inelastic electron and muon  $\mathcal{F}_2$  data on proton and deuteron targets are shown in Figures 2 (for SLAC, BCDMS and NMC). Comparisons to low  $x$  H1(electron) data on protons are shown in Figure 3. Our effective LO model describes the inelastic charged lepton  $\mathcal{F}_2$  data both in the low  $x$  as well as in the high  $x$  regions. The model also provides a good description of both low energy and high energy photo-production cross sections[32] on proton and deuteron targets as shown in Figure 6.

### 5. Comparison to resonance production data

Comparisons of the model fit to hydrogen and deuterium electron scattering data in the resonance region [33] are shown in Figure 4. As expected from quark-hadron duality [36], our model provides a reasonable description of both the inelastic region as well as the average value of the  $\mathcal{F}_2$  data in the resonance region (down to  $Q^2 = 0$ ), including the region of the first resonance ( $W = 1.23 \text{ GeV}/c^2$ ). We find also good agreement with the most recent  $\mathcal{F}_L$  and  $\mathcal{F}_2$  data in the resonance region from the E94-110, and JUPITER experiments [33,37] at Jlab, as shown in Fig. 5. Our predictions for  $\mathcal{F}_L$  are obtained using our  $\mathcal{F}_2$  model and the  $R_{1998}$  [38] parametrization (as discussed in section 9). We find good agreement with quark hadron duality down to very low  $Q^2$ . Other studies[30] with unmodified GRV PDFs find large deviations from quark-hadron duality in the resonance region for electron and muon scattering. This is because those studies do not include any low  $Q^2$   $K$  factors and

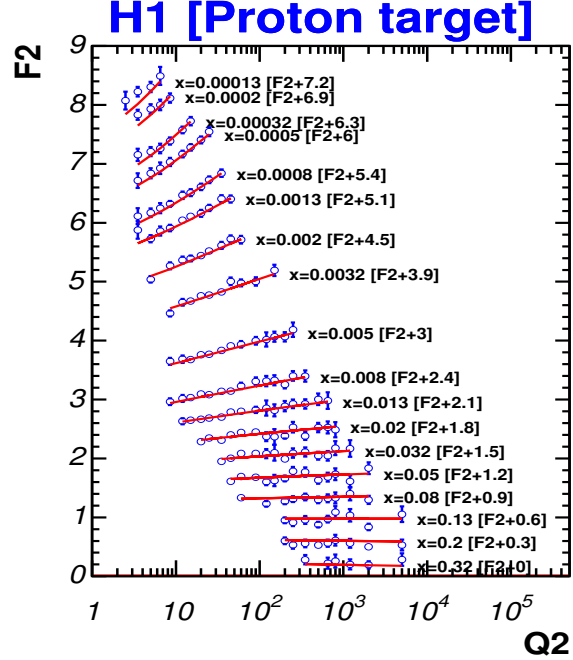


Figure 3. The effective LO PDF model compared to charged lepton  $\mathcal{F}_2$  experimental data at low  $x$  from H1 (these data are included in our fit).

use the scaling variable  $\xi$  (while we use the modified scaling variable  $\xi_w$ ). We find that quark hadron duality works at low  $Q^2$  if we use the modified scaling variable  $\xi_w$ , and low  $Q^2$   $K_i$  factors.

In the  $Q^2 = 0$  photoproduction limit, the model provides a good descriptions of the data for both the inelastic region as well as in the resonance region as shown in Figure 6. Since the photoproduction cross sections on protons and neutrons are not far apart, our fits yield the interesting result that at  $Q^2 = 0$ , the effective valence  $d$  quark is multiplied by a factor of 0.85 ( $=0.323/0.341$ ), and the effective valence  $u$  quark distribution at  $Q^2 = 0$  is multiplied by a factor of 0.634 ( $=0.264/0.417$ ). This implies that at  $Q^2 = 0$ , the effective  $d/u$  ratio for valence quark is enhanced by a factor of 1.5.

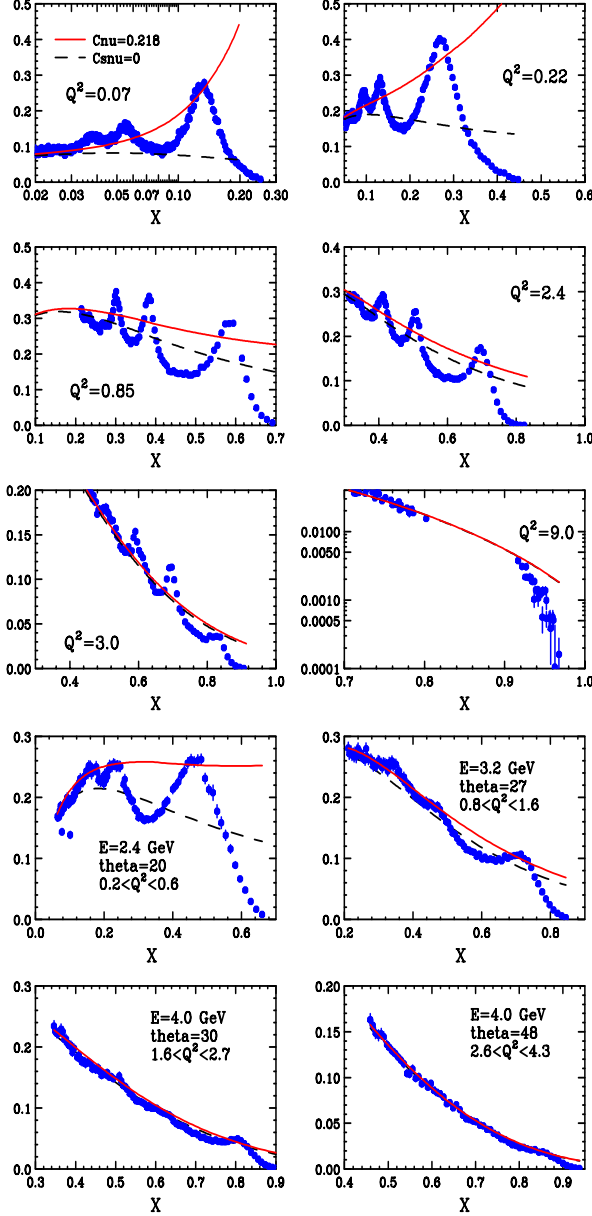


Figure 4. Comparisons of charged lepton experimental data in the resonance region to the predictions of our effective LO model: [top] six proton plots, [bot] four deuteron pots. The red line includes the  $K^{LW}$  factor and the dashed black line does not include the  $K^{LW}$  factor. Note that the  $K^{LW}$  factor is not used in the region of the  $\Delta(1232)$  resonance.

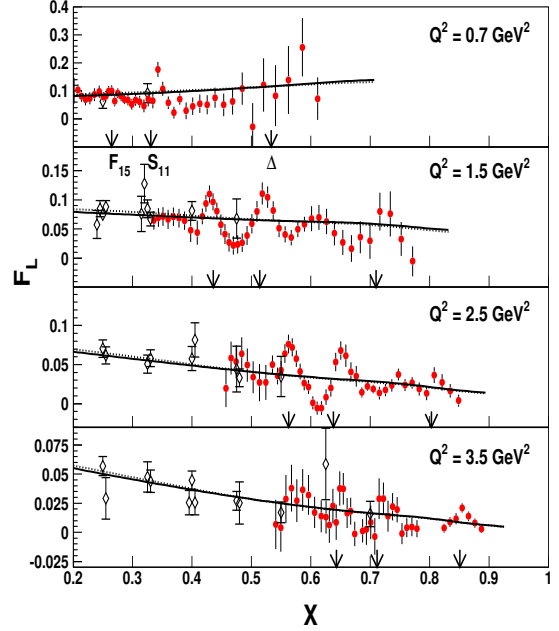


Figure 5. Comparisons of the predictions of our model to proton data for  $\mathcal{F}_L$  (note that data for  $\mathcal{F}_L$  are not included in our fit).

## 6. Application to neutrino scattering

For high energy neutrino scattering on quarks and antiquarks, the vector and axial contributions are the same. At very high  $Q^2$ , where the quark parton model is valid, both the vector and axial  $K$  factors are expected to be 1.0. Therefore, high  $Q^2$  neutrinos and antineutrino structure functions are given by :

$$\mathcal{F}_2^\nu(x, Q^2) = 2\Sigma_i [\xi_w q_i(\xi_w, Q^2) + \xi_w \bar{q}_i(\xi_w, Q^2)] .$$

and

$$x\mathcal{F}_3^\nu(x, Q^2) = 2\Sigma_i [\xi_w q_i(\xi_w, Q^2) - \xi_w \bar{q}_i(\xi_w, Q^2)] .$$



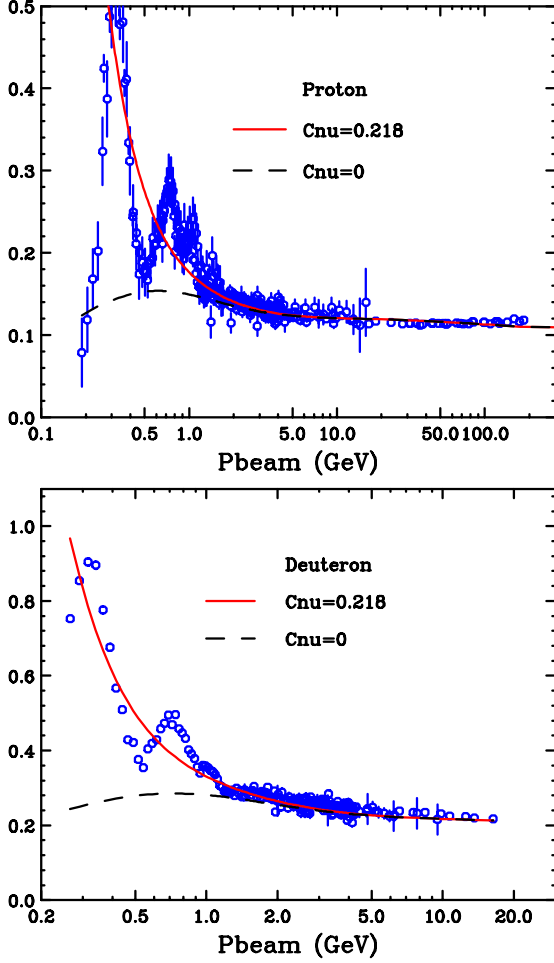


Figure 6. The effective LO PDF model compared to photoproduction cross sections ( $Q^2 = 0$  limit) at low and high energies (these data are included in our fit). [top] proton, [bot] deuteron. At very high photon energy, we include charm contribution from gluon fusion process which is needed to describe the very high energy HERA data. If we want to also describe the photoproduction data in the resonance region, we need to multiply the  $u$  and  $d$  valence PDFs by  $K^{LW} = (\nu^2 + C^{L-Ehad})/(\nu^2 + 2Q^2)$ . The red line includes the  $K^{LW}$  factor, and the dashed black line does not include the  $K^{LW}$  factor. Note that the  $K^{LW}$  factor is not used in the region of the  $\Delta(1232)$  resonance.

where

$$\begin{aligned}
 q^{\nu p} &= d + s; & \bar{q}^{\nu p} &= \bar{u} + \bar{c} \\
 q^{\nu n} &= u + s; & \bar{q}^{\nu p} &= \bar{d} + \bar{c} \\
 q^{\bar{\nu} p} &= u + c; & \bar{q}^{\nu p} &= \bar{d} + \bar{s} \\
 q^{\bar{\nu} n} &= d + c; & \bar{q}^{\nu p} &= \bar{u} + \bar{s}
 \end{aligned} \tag{21}$$

Here,  $\mathcal{F}_2 = \nu\mathcal{W}_2$ ,  $\mathcal{F}_1 = M\mathcal{W}_1$  and  $\mathcal{F}_3 = \nu\mathcal{W}_3$ . Note that for the strangeness conserving ( $sc$ ) part of the  $u$  and  $d$  quark distributions, the PDFs are multiplied by a factor of  $\cos^2\theta_c$ . For the strangeness non-conserving part the PDFs are multiplied by a factor of  $\sin^2\theta_c$ .

The neutrino structure functions must satisfy the following inequalities:

$$\begin{aligned}
 0 &\leq \sqrt{Q^2 + \nu^2} \frac{|\mathcal{W}_3|}{2M} \\
 \mathcal{W}_1 &\geq \sqrt{Q^2 + \nu^2} \frac{|\mathcal{W}_3|}{2M} \\
 \mathcal{W}_1 &\leq (1 + \nu^2/Q^2)\mathcal{W}_2
 \end{aligned} \tag{22}$$

There are several major difference between the case of charged lepton inelastic scattering and the case of neutrino scattering. In the neutrino case we have one additional structure functions  $\mathcal{F}_3^\nu(x, Q^2)$ . In addition, at low  $Q^2$  there should be a difference between the vector and axial  $K_i$  factors due a difference in the non-perturbative axial vector contributions. Unlike the vector  $\mathcal{F}_2$  which must go to zero in the  $Q^2 = 0$  limit, we expect [24,40] that the axial part of  $\mathcal{F}_2$  is non-zero in the  $Q^2 = 0$  limit.

We already account for kinematic and dynamic higher twist and higher order QCD effects in  $\mathcal{F}_2$  by fitting the parameters of the scaling variable  $\xi_w$  and the  $K$  factors to low  $Q^2$  data for  $\mathcal{F}_2^e\mu(x, Q^2)$ . These should also be valid for the vector part of  $\mathcal{F}_2$  in neutrino scattering. However, the higher order QCD effects in  $\mathcal{F}_2$  and  $x\mathcal{F}_3$  are different. We account for the different scaling violations in  $\mathcal{F}_2$  and  $x\mathcal{F}_3$  by adding a correction factor  $H(x, Q^2)$ .

The axial  $K$  factors and the  $H$  correction to  $x\mathcal{F}_3$  are included in the following expressions:

$$\begin{aligned}
 \mathcal{F}_2^{\nu vector}(x, Q^2) &= \sum_i K_i^{vector}(Q^2)\xi_w q_i(\xi_w, Q^2) \\
 &\quad + \sum_j K_j^{vector}(Q^2)\xi_w \bar{q}_j(\xi_w, Q^2)
 \end{aligned} \tag{23}$$

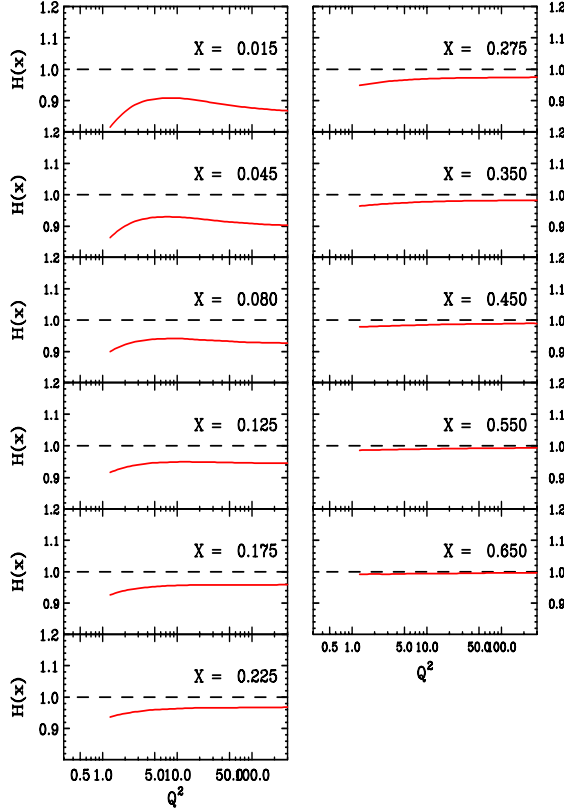


Figure 7. The  $x$  and  $Q^2$  dependence of the factor  $H(x, Q^2)$  that accounts for the difference in the QCD higher order corrections in  $\mathcal{F}_2$  and  $x\mathcal{F}_3$

and

$$\mathcal{F}_2^{\nu axial}(x, Q^2) = \sum_i K_i^{axial}(Q^2) \xi_w q_i(\xi_w, Q^2) + \sum_j K_j^{axial}(Q^2) \xi_w \bar{q}_j(\xi_w, Q^2) \quad (24)$$

and

$$x\mathcal{F}_3^{\nu}(x, Q^2) = 2H(x, Q^2) \left\{ \sum_i K_i^{xF3} \xi_w q_i(\xi_w, Q^2) - \sum_j K_j^{xF3} \xi_w \bar{q}_j(\xi_w, Q^2) \right\} \quad (25)$$

where,  $i$  denotes (*valence - up*), (*valence - down*), (*sea - up*), (*sea - down*), and (*sea -*

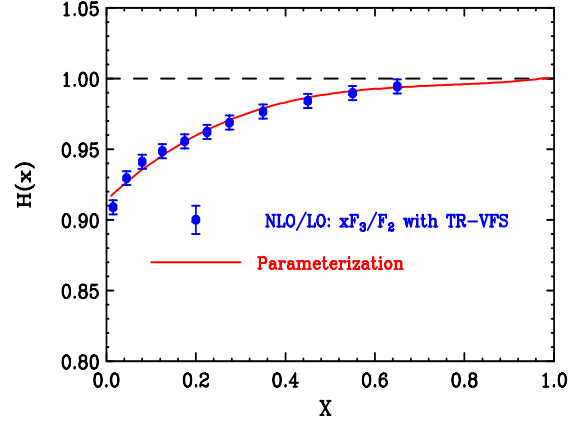


Figure 8. A fit to the  $x$  dependence of the factor  $H(x, Q^2)$  that accounts for the difference in the QCD higher order corrections in  $\mathcal{F}_2$  and  $x\mathcal{F}_3$  (at  $Q^2 = 8 \text{ (GeV/c)}^2$ ).

*strange*), and  $j$  denotes (*sea - up*), (*sea - down*), and (*sea - strange*). The factor  $K_i^{xF3}$  is given by

$$K_i^{xF3} = \sqrt{\frac{Q^2 K_i^{axial}(Q^2) K_i^{vector}(Q^2)}{Q^2 + C_{xF3}}} \quad (26)$$

The parameter  $C_{xF3} = 0.33$  is set such that the Adler sum rule for  $x\mathcal{F}_3$  is satisfied at  $Q^2 = 0$ .

We obtain an approximate expression for  $H(x, Q^2)$  as the ratio of two ratios as follows:  $H(x, Q^2) = D_{xF3}(x, Q^2) / D_{F2}(x, Q^2)$  where

$$\begin{aligned} D_{xF3}(x, Q^2) &= \frac{x\mathcal{F}_3^{nlo}(x, Q^2)}{x\mathcal{F}_3^{lo}(x, Q^2)} \\ D_{F2}(x, Q^2) &= \frac{\mathcal{F}_2^{nlo}(x, Q^2)}{\mathcal{F}_2^{lo}(x, Q^2)} \end{aligned} \quad (27)$$

The double ratio  $H(x, Q^2)$  is calculated by the TR-VFS scheme[39] with MRST991 NLO PDFs. This ratio turns out to be almost independent of  $Q^2$ . The results of this calculation at  $Q^2 = 8(\text{GeV/c})^2$  are fit by the following functional form:

$$\begin{aligned} H(x, Q^2) &= 0.914 + 0.296x \\ &- 0.374x^2 + 0.165x^3 \end{aligned} \quad (28)$$

We use the above function as an approximation for  $H(x, Q^2)$  for all values of  $Q^2$ .

In our previous [10,11] analysis we assumed  $H(x, Q^2)=1$ ,  $C_{xF3} = 0$ , and  $K_i^{axial}(Q^2)=K_i^{vector}(Q^2)$ . However, this assumption is only valid for  $Q^2 > 1 \text{ (GeV/c)}^2$ . Here, we improve on our previous analysis by introducing  $K_i^{axial}(Q^2)$  factors which are different from  $K_i^{vector}(Q^2)$ , and include the  $H(x, Q^2)$  and  $C_{xF3}$  corrections for  $x\mathcal{F}_3$ .

## 7. Axial structure function $\mathcal{F}_2$ , and the structure function $x\mathcal{F}_3$

The axial structure function  $\mathcal{F}_2$  is not constrained to go to zero at  $Q^2 = 0$ . At higher  $Q^2$  (e.g.  $Q^2 \geq 1$ ) the vector and axial structure functions should be equal.

The simplest assumption to make is that for valence quarks the parameters of parton distributions and associated  $K$  factors for the axial case are the same as the parameters for the vector case, except for the parts that constrain  $\mathcal{F}_2$  to be zero at  $Q^2$ . Here, we assume that the axial  $K$  factor for valence quarks is equal to 1 (versus the vector valence  $K$  factor which is  $(1 - G_D(Q^2))$ ).

Therefore, the suggested axial  $K$  factors are:

$$\begin{aligned} K_{\nu d}^{LW} &= \frac{\nu^2 + C^{L-Ehad}}{\nu^2} \quad (W > 1.4 \text{ GeV/c}^2) \\ K_{\nu u}^{LW} &= \frac{\nu^2 + C^{L-Ehad}}{\nu^2} \quad (W > 1.4 \text{ GeV/c}^2) \\ K_{\nu d}^{LW} &= K_{\nu-d}^{\Delta 1232} = 1.65 \quad (W < 1.4 \text{ GeV/c}^2) \\ K_{\nu u}^{LW} &= K_{\nu-u}^{\Delta 1232} = 0.55 \quad (W < 1.4 \text{ GeV/c}^2) \end{aligned} \quad (29)$$

and

$$\begin{aligned} K_{valence-down}^{axial}(Q^2) &= K_{\nu d}^{LW} \left( \frac{Q^2 + C_{v2d}^{vector}}{Q^2 + C_{v1d}^{vector}} \right) \\ K_{valence-up}^{axial}(Q^2) &= K_{\nu u}^{LW} \left( \frac{Q^2 + C_{v2u}^{vector}}{Q^2 + C_{v1u}^{vector}} \right) \end{aligned}$$

For sea quarks, we need to include additional parameters

$$\begin{aligned} K_{sea-strange}^{axial}(Q^2) &= \frac{Q^2 + P_s C_{sea-strange}^{axial}}{Q^2 + C_{sea-strange}^{axial}} \\ K_{sea-down}^{axial}(Q^2) &= \frac{Q^2 + P_d C_{sea-down}^{axial}}{Q^2 + C_{sea-down}^{axial}} \\ K_{sea-up}^{axial}(Q^2) &= \frac{Q^2 + P_u C_{sea-up}^{axial}}{Q^2 + C_{sea-up}^{axial}} \end{aligned} \quad (30)$$

In addition, as mentioned earlier

$$K_i^{xF3} = \sqrt{\frac{Q^2 K_i^{axial}(Q^2) K_i^{vector}(Q^2)}{Q^2 + C_{xF3}}} \quad (31)$$

where the parameter  $C_{xF3} = 0.33$ . With this value, we get that  $\mathcal{W}_3(Q^2 = 0)$  for the  $\Delta$  (1232) is equal to 11. This is close to the theoretical calculation of Lalakulich and Paschos[34]. In addition, with this value the Adler rule for  $x\mathcal{F}_3$  is approximately satisfied at  $Q^2 = 0$ .

We make the following assumptions

$$\begin{aligned} P = P_u = P_d = P_s &= 0.6 \pm 0.3 \\ C_{sea-strange}^{axial} &= 0.3 \\ C_{sea-down}^{axial} &= 0.3 \\ C_{sea-up}^{axial} &= 0.3 \end{aligned} \quad (32)$$

With these choices the axial  $K$  factors are between  $K = 1$  ( $P=1$ ) and  $K^{axial} = K^{vector}$ . Here  $P = 0.6 \pm 0.3$  yields  $\mathcal{F}_2^{axial}(\xi_w = 0.00001, Q^2 = 0)_{(p+n)/2} = 0.33 \pm 0.16$  for the average of the neutron and proton structure functions, which is the value calculated from PCAC in the model of Kulagin and Peti[40]. For an iron target (assuming a ratio  $Fe/D = 0.8$ ) this corresponds to  $\mathcal{F}_2^{axial}(\xi_w = 0.00001, Q^2 = 0)_{Fe} = 0.25 \pm 0.11$ , which is similar with the value of  $0.210 \pm 0.02$  measured by CCFR [25] using a different functional form for the extrapolation of their data to  $Q^2 = 0$ . The value of  $C_{sea}^{axial} = 0.3$  was selected because it yields a PCAC contribution for  $\mathcal{F}_2^{axial}(\xi_w = 0.00001, Q^2 = 1) = 0.08$ , which is the value calculated in the model of Kulagin and Peti[40].

A better determination of the axial  $K$  factors for the sea quarks requires including neutrino data on nuclear targets in our fit. The nuclear

corrections at small  $x$  for vector and axial structure functions are different in general. Therefore, it is not possible to separately determining the axial  $K$  factor without assuming a specific model for the neutrino nuclear corrections[40]. Therefore, this study will be presented in a future communication.

### 8. Comparison to neutrino and antineutrino data on the production of the $\Delta$ 1232 Resonance

Our model is aimed at describing neutrino cross sections in the inelastic region (e.g.  $W > 1.9 \text{ GeV}/c^2$ ) and match on to other calculations[34,35] that describe the resonance region and the quasielastic peak. In order to match smoothly to a resonance region model, the model should also describe the average of the cross section in the resonance region. Since the model describes electron and muon scattering structure functions in the resonance region (on average, as expected from local duality), it should also work for the vector part of the structure functions in neutrino scattering.

We now test how well the suggested axial parameters for the valence quarks describe the production of the  $\Delta(1232)$  resonances on proton and neutron targets.

At a fixed value of the final state invariant mass  $W$ , the differential cross section for neutrino scattering at incident energy  $E$  is given[30] by:

$$\begin{aligned} \frac{d\sigma}{dQ^2 dW} = \frac{G^2}{4\pi} \cos^2 \theta_C \frac{W}{ME^2} & \left\{ \mathcal{W}_1(Q^2 + m_\mu^2) \right. \\ & + \frac{\mathcal{W}_2}{M^2} \left[ 2(k \cdot p)(k' \cdot p) - \frac{1}{2} M^2(Q^2 + m_\mu^2) \right] \\ & + \frac{\mathcal{W}_3}{M^2} \left[ Q^2 k \cdot p - \frac{1}{2} q \cdot p(Q^2 + m_\mu^2) \right] \\ & \left. + \frac{\mathcal{W}_4}{M^2} m_\mu^2 \frac{(Q^2 + m_\mu^2)}{2} - 2 \frac{\mathcal{W}_5}{M^2} m_\mu^2 (k \cdot p) \right\} \end{aligned} \quad (33)$$

where  $k$  and  $k'$  are the momenta of the initial and final state lepton, and  $p$  is the momentum of the

target nucleon. This expression can be written as

$$\begin{aligned} \frac{d\sigma}{dQ^2 dW} = \frac{G^2}{4\pi} \cos^2 \theta_C \frac{W}{M} & \left\{ \frac{1}{E^2} \mathcal{W}_1(Q^2 + m_\mu^2) \right. \\ & + \mathcal{W}_2 \left[ 2\left(1 - \frac{\nu}{E}\right) - \frac{1}{2E^2}(Q^2 + m_\mu^2) \right] \\ & + \mathcal{W}_3 \left[ \frac{Q^2}{ME} - \frac{\nu}{2E} \frac{Q^2 + m_\mu^2}{ME} \right] \\ & \left. + \frac{\mathcal{W}_4}{M^2} m_\mu^2 \frac{(Q^2 + m_\mu^2)}{2E^2} - 2 \frac{\mathcal{W}_5}{ME} m_\mu^2 \right\} \end{aligned} \quad (34)$$

vector part of  $\mathcal{W}_4$  and  $\mathcal{W}_5$  are related to the vector part of  $\mathcal{W}_2$  and  $\mathcal{W}_1$  by the following expressions[34]:

$$\begin{aligned} \mathcal{W}_4^{vector} &= \mathcal{W}_2^{vector} \frac{M\nu}{Q^2} \\ \mathcal{W}_5^{vector} &= \mathcal{W}_2^{vector} \frac{M^2\nu^2}{Q^4} - \mathcal{W}_1 \frac{M^2}{Q^2} \end{aligned} \quad (35)$$

The contribution of the  $\mathcal{W}_4$  and  $\mathcal{W}_5$  should be accounted for in the case of  $\tau$  neutrino interactions[41]. For muon neutrinos, we find that even for a neutrino energy as low as  $1 \text{ GeV}$ , the contribution of the  $\mathcal{W}_4$  term is negligible. Using the model of O. Lalakulich, E. A. Paschos for the production of the  $\Delta(1232)$  resonance[34] we find that for a neutrino energy of  $1 \text{ GeV}$ , the contribution of the  $\mathcal{W}_5$  term is about 10% for  $Q^2$  close to  $m_\mu^2$ . We also find that the assumption  $\mathcal{W}_4^{axial} = \mathcal{W}_4^{vector}$ , and  $\mathcal{W}_5^{axial} = \mathcal{W}_5^{vector}$  is good to within 30% for  $Q^2 = 0$ .

At high energy ( $E > 20 \text{ GeV}$ ), for low values of  $W$  (for which  $\nu$  is small) and low  $Q^2$  ( $Q^2 < 3 (\text{GeV}/c)^2$ ), all the terms are small except for  $\mathcal{W}_2$  term. For this case the above expression reduces to :

$$\begin{aligned} \frac{d\sigma^{\nu N \rightarrow \Delta}}{dQ^2 dW} &= \frac{G^2}{2\pi} \cos^2 \theta_C \frac{W}{M} \frac{\mathcal{F}_2^{\nu N \rightarrow \Delta}}{\nu}(W, Q^2) \\ &= S_{cos} \frac{W}{M} \frac{\mathcal{F}_2^{\nu N \rightarrow \Delta}}{\nu}(W, Q^2) \end{aligned} \quad (36)$$

where  $S_{cos} = \frac{G^2}{2\pi} \cos^2 \theta_C = 80 \times 10^{-40} \text{ cm}^2$ , and  $\mathcal{F}_2^{\nu N \rightarrow \Delta}$  is the average value of  $\mathcal{F}_2$  in the region of the  $\Delta(1232)$  resonance ( $1.1 < W < 1.4 \text{ GeV}/c^2$ ).

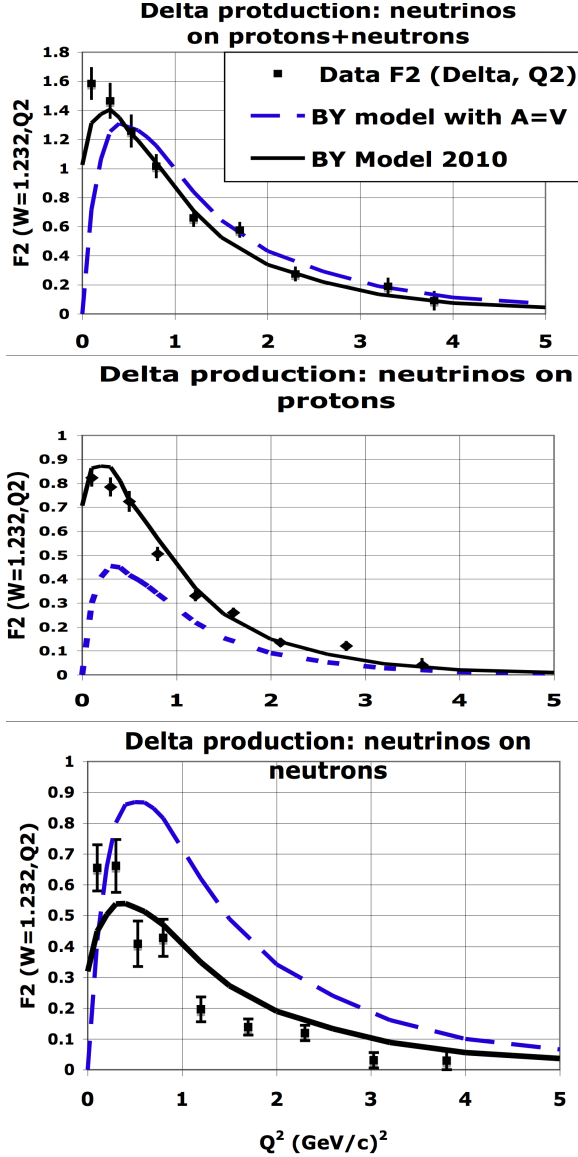


Figure 9. A comparison of  $\mathcal{F}_2^{\nu p \rightarrow \Delta}(Q^2)$ ,  $\mathcal{F}_2^{\nu n \rightarrow \Delta}(Q^2)$  and the sum  $\mathcal{F}_2^{\nu(p+n) \rightarrow \Delta}(Q^2)$  extracted from  $\Delta$  production data to our predictions. Solid line, our updated model with suggested axial parameters, and  $K_{\nu-u}^{\Delta 1232} = 0.55$  and  $K_{\nu-d}^{\Delta 1232} = 1.65$ . The dashed blue line is predictions of our model with the assumptions of Axial=Vector and  $K_{\nu-u}^{\Delta 1232} = 1$  and  $K_{\nu-d}^{\Delta 1232} = 1$ .

For a specified range of the final state invariant mass  $\delta_W$  we get.

$$\mathcal{F}_2^{\nu p \rightarrow \Delta}(Q^2) = \frac{\nu M}{S_{cos} W \delta_W} \frac{d\sigma^{\nu p \rightarrow \Delta}}{dQ^2} \quad (37)$$

and

$$\mathcal{F}_2^{\nu n \rightarrow \Delta}(Q^2) = \frac{\nu M}{S_{cos} W \delta_W} \frac{d\sigma^{\nu n \rightarrow \Delta}}{dQ^2} \quad (38)$$

For the region of the  $\Delta(1232)$  resonance  $W = 1.23 \text{ GeV}/c^2$ , and  $\delta_W = 0.3 \text{ GeV}/c^2$ , which corresponds to the invariant mass range from pion threshold  $M_\pi + M = 1.1 \text{ GeV}/c^2$  to  $1.4 \text{ GeV}/c^2$ .

The antineutrino structure functions are related to the neutrino structure functions by the following relations.

$$\begin{aligned} \mathcal{F}_i^{\bar{\nu} p} &= \mathcal{F}_i^{\nu n} \\ \mathcal{F}_i^{\bar{\nu} n} &= \mathcal{F}_i^{\nu p} \end{aligned} \quad (39)$$

For  $d\sigma^{\nu p \rightarrow \Delta}/dQ^2$  in the  $1.1 < W < 1.4 \text{ GeV}/c^2$  region we take the average of  $d\sigma^{\nu p \rightarrow p\pi^+}/dQ^2$  data of Allen *et al* [42] and Allasia *et al* [43]. Since  $\mathcal{F}_i^{\bar{\nu} p} = \mathcal{F}_i^{\nu n}$  we also include the Allasia *et al* data for  $d\sigma^{\bar{\nu} n \rightarrow n\pi^-}/dQ^2$  in this average. For  $d\sigma^{\nu n \rightarrow \Delta}/dQ^2$  data we sum the Allasia *et al* measurements for  $d\sigma^{\nu n \rightarrow p\pi^0}/dQ^2$  and the  $d\sigma^{\nu n \rightarrow n\pi^+}/dQ^2$  measurements in the  $1.1 < W < 1.4 \text{ GeV}/c^2$  region.

Figure 9 shows a comparison data for  $\mathcal{F}_2^{\nu p \rightarrow \Delta}(W = 1.23, Q^2)$ ,  $\mathcal{F}_2^{\nu n \rightarrow \Delta}(W = 1.23, Q^2)$  and for the sum  $\mathcal{F}_2^{\nu(p+n) \rightarrow \Delta}(W = 1.23, Q^2)$ , extracted from the Allen *et al* [42] and Allasia *et al* [43] measurements, to our predictions (with  $K_{\nu-u}^{\Delta 1232} = 0.55$  and  $K_{\nu-d}^{\Delta 1232} = 1.65$ ). There is good agreement between the  $\Delta$  production data and our model.

Also shown is the predictions of our model under the assumption that Axial=Vector and  $K_{\nu-u}^{\Delta 1232} = 1$  and  $K_{\nu-d}^{\Delta 1232} = 1$ . Using the suggested axial parameters yields a better description of the data near  $Q^2 = 0$ , and also a better description of the difference between the scattering on protons and neutrons.

For most applications the target consists of approximately equal numbers of neutrons and protons. For such isoscalar targets, our previous version which assumed that Axial=Vector and

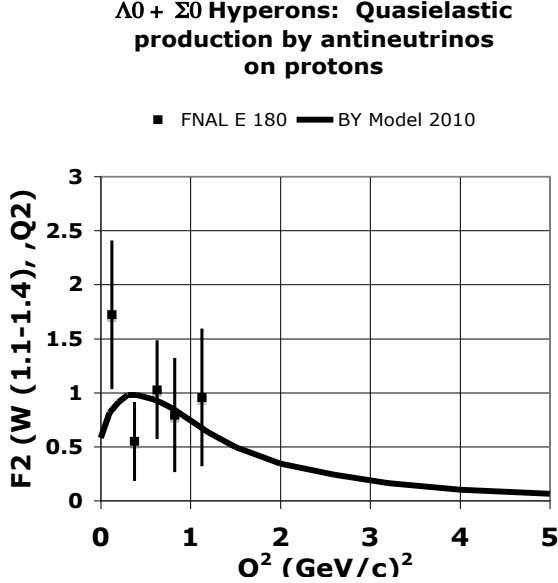


Figure 10. A comparison data for  $\mathcal{F}_2^{\bar{\nu}p \rightarrow \Lambda_0, \Xi_0}$  extracted from the measured differential cross section for hyperon production from Fermilab experiment E180 [44] to our predictions with  $K^{LW}(W < 1.4) = 1$ . There is good agreement between the  $\Lambda_0, \Xi_0$  production data and our model.

$K_{\nu-u}^{\Delta 1232} = 1$  and  $K_{\nu-d}^{\Delta 1232} = 1$ . worked reasonably well except near  $Q^2 = 0$ . Our model with updated axial parameters works much better.

### 9. Comparison to quasielastic production of the $\Lambda_0$ and $\Xi_0$ hyperon resonances.

The expression for quasielastic production of  $\Lambda_0(1116)$  and  $\Xi_0(1193)$  hyperon  $uds$  resonances in antineutrino-proton collisions is given by:

$$\begin{aligned} \frac{d\sigma^{\bar{\nu}p \rightarrow \Lambda_0, \Xi_0}}{dQ^2 dW} &= \frac{G^2}{2\pi} \sin^2 \theta_C \frac{W}{M} \frac{\mathcal{F}_2^{\bar{\nu}p \rightarrow \Lambda_0, \Xi_0}}{\nu}(Q^2) \\ &= S_{sin} \frac{W}{M} \frac{\mathcal{F}_2^{\bar{\nu}p \rightarrow \Lambda_0, \Xi_0}}{\nu}(Q^2) \end{aligned} \quad (40)$$

$$\mathcal{F}_2^{\bar{\nu}p \rightarrow \Lambda_0, \Xi_0}(Q^2) = \frac{\nu M}{S_{sin} W \delta_W} \frac{d\sigma^{\bar{\nu}p \rightarrow \Lambda_0, \Xi_0}}{dQ^2} \quad (41)$$

where  $S_{sin} = \frac{G^2}{2\pi} \sin^2 \theta_C = 4.29 \times 10^{-40} \text{ cm}^2$ . Here,  $\mathcal{F}_2$  is the average value of  $\mathcal{F}_2$  for the range  $1.1 < W < 1.4 \text{ GeV}/c^2$ , where  $1.4 \text{ GeV}/c^2$  is the proton-kaon threshold, and  $\delta_w = 0.3 \text{ GeV}/c^2$ . Therefore, in the expressions are identical to the expressions for the production of the  $\Delta 1232$ , except that here we have  $\sin^2 \theta_C$  instead of  $\cos^2 \theta_C$ . Since we do not have a  $I = 3/2$  resonance, we use  $K^{LW}(1.1 < W < 1.4) = 1$ .

Figure 10 shows a comparison of data for  $\mathcal{F}_2^{\bar{\nu}p \rightarrow \Lambda_0, \Xi_0}$  extracted from the measured differential cross section for hyperon production from Fermilab experiment E180 [44] to our predictions with  $K^{LW}(W < 1.4) = 1$ . There is good agreement between the hyperon ( $\Lambda_0, \Xi_0$ ) production data and our model.

### 10. $2x\mathcal{F}_1^{vector}$ and the longitudinal structure function

In the extraction of the original GRV98 LO PDFs, no separate longitudinal contribution was included. The quark distributions were directly fit to  $\mathcal{F}_2$  data. A full modeling of electron and muon cross section requires also a description of  $2x\mathcal{F}_1$ . We use a non-zero longitudinal  $R$  in reconstructing  $2x\mathcal{F}_1$  by using a fit of  $R$  to measured data. In general,  $2x\mathcal{F}_1^{e/\mu}$  is given by

$$2x\mathcal{F}_1^{e/\mu}(x, Q^2) = \mathcal{F}_2^{e/\mu}(x, Q^2) \times \frac{1 + 4M^2 x^2 / Q^2}{1 + R(x, Q^2)} \quad (42)$$

or equivalently

$$\mathcal{W}_1^{e/\mu}(x, Q^2) = \mathcal{W}_2^{e/\mu}(x, Q^2) \times \frac{1 + \nu^2 / Q^2}{1 + R(x, Q^2)} \quad (43)$$

The  $R_{1998}$  function[38] provides a good description of the world's data for  $R$  in the  $Q^2 > 0.30 \text{ (GeV}/c^2)$  and  $x > 0.05$  region (where most of the

$R$  data are available).

$$R_{e/\mu}(x, Q^2 > 0.3) = R_{1998}(x, Q^2 > 0.3) \quad (44)$$

However, for electron and muon scattering (and for the vector part of neutrino scattering) the  $R_{1998}$  function breaks down below  $Q^2 = 0.3$  ( $\text{Gev}/c^2$ ). Therefore, we freeze the function at  $Q^2 = 0.3$  ( $\text{Gev}/c^2$ ) and introduce additional parameters for  $R$  in the  $Q^2 < 0.3$  ( $\text{Gev}/c^2$ ) region. For electron and muon scattering and for the vector part of  $\mathcal{F}_1$  we introduce a  $K$  factor for  $R$  in the  $Q^2 < 0.3$  ( $\text{Gev}/c^2$ ) region. The new function provides a smooth transition for  $R_{e/\mu}$  from  $Q^2 = 0.3$  ( $\text{Gev}/c^2$ ) down to  $Q^2 = 0$  by forcing  $R_{vector}$  to approach zero at  $Q^2 = 0$  as expected in the photoproduction limit. This procedure keeps a  $1/Q^2$  behavior at large  $Q^2$  and matches to  $R_{1998}$  at  $Q^2 = 0.3$  ( $\text{Gev}/c^2$ ).

$$R_{e/\mu}(x, Q^2 < 0.3) = 3.633 \times \frac{Q^2}{Q^4 + 1} \times R_{1998}(x, Q^2 = 0.3)$$

Using the above fits to  $R$  as measured in electron/muon scattering we use the following expressions for the vector part of  $2x\mathcal{F}_1$  neutrino scattering.

$$\begin{aligned} 2x\mathcal{F}_1^{vector}(x, Q^2) &= \mathcal{F}_2^{vector}(x, Q^2) \times \frac{1 + 4M^2x^2/Q^2}{1 + R(x, Q^2)} \\ R_{vector}(x, Q^2 > 0.3) &= R_{1998}(x, Q^2 > 0.3) \\ R_{vector}(x, Q^2 < 0.3) &= R_{e/\mu}(x, Q^2 < 0.3) \end{aligned}$$

or equivalently

$$\mathcal{W}_1^{vector}(x, Q^2) = \mathcal{W}_2^{vector}(x, Q^2) \times \frac{1 + \nu^2/Q^2}{1 + R_{vector}(x, Q^2)} \quad (45)$$

The above expressions have the correct limit at  $Q^2 = 0$ .

## 11. The structure function $2x\mathcal{F}_1^{axial}$

As is the case for  $\mathcal{F}_2 = \nu\mathcal{W}_2$ , the axial component of  $2x\mathcal{F}_1$  ( $= 2xM\mathcal{W}_1$ ) at large  $Q^2$  is equal

to the vector component of  $2x\mathcal{F}_1$ . Investigation of the Adler sum rules (described in section 15) shows that at  $Q^2 = 0$ , the Adler sum rules for the axial structure functions  $\mathcal{W}_1^{axial}$  and  $\mathcal{W}_2^{axial}$  are the same.

Therefore, we assume that  $\mathcal{W}_1^{axial}(Q^2 = 0) = \mathcal{W}_2^{axial}(Q^2 = 0)$ . This also implies that the longitudinal part of  $\mathcal{W}_2^{axial}$  dominates at  $Q^2 = 0$  as expected from PCAC[40]. Here, since  $\mathcal{F}_2^{axial}(Q^2 = 0)$  is non zero, it implies that  $R^{axial}(Q^2 = 0)$  is infinite. Therefore, it is more convenient to calculate  $\mathcal{W}_1^{axial}$  instead of  $\mathcal{F}_1^{axial}$  at low  $Q^2$ .

In summary, at large  $Q^2$  we expect:

$$\mathcal{W}_1^{axial}(x, Q^2 > 1) = \mathcal{W}_1^{vector}(x, Q^2)$$

And at  $Q^2 = 0$  we expect:

$$\mathcal{W}_1^{axial}(x, Q^2 = 0) = \mathcal{W}_2^{axial}(x, Q^2)$$

We use a function for  $\mathcal{W}_1^{axial}$  that matches these two boundary conditions as follows.

$$\begin{aligned} \mathcal{W}_1^{axial}(x, Q^2) &= \mathcal{W}_1^{vector}(x, Q^2) \frac{Q^2}{Q^2 + 0.2} \\ &+ \mathcal{W}_2^{axial}(x, Q^2) \left(1 - \frac{Q^2}{Q^2 + 0.2}\right) \end{aligned} \quad (46)$$

## 12. Charm production in neutrino scattering

Neutrino scattering is not as simple as the case of charged lepton scattering because of charm production. For the non-charm production components we use  $\mathcal{F}_2^{ncp}(x, Q^2)$ ,  $2x\mathcal{F}_1^{ncp}(x, Q^2)$  (sum of vector and axial parts) and  $x\mathcal{F}_3^{ncp}(x, Q^2)$  as described above.

For the charm production components of  $\mathcal{F}_2^{cp}(x, Q^2)$ ,  $x\mathcal{F}_3^{cp}(x, Q^2)$  and  $2x\mathcal{F}_1^{cp}(x, Q^2)$  the variable  $\xi_w$  now includes a non-zero  $M_c = 1.32\text{GeV}/c^2$ .

The target mass calculations as discussed by Barbieri et. al[22] imply that  $\mathcal{F}_2^{\nu-cp}$  is described by  $\mathcal{F}_2^{\nu-cp}(\xi_w, Q^2)$ , and the other two structure functions are multiplied by the factor  $K_{charm} = \frac{Q^2}{Q^2 + M_c^2}$ . Therefore, to include charm production we use the following expression for charm production processes.

$$\begin{aligned}
K_{charm} &= \frac{Q^2}{Q^2 + M_C^2} \\
\mathcal{F}_2^{\nu, vector-cp}(x, Q^2) &= \Sigma_i K_i^{vector}(Q^2) \\
&\times [\xi_w q_i(\xi_w, Q^2) + \xi_w \bar{q}_i(\xi_w, Q^2)] \\
\mathcal{F}_2^{\nu, axial-cp}(x, Q^2) &= \Sigma_i [K_i^{axial}(Q^2) \\
&\times [\xi_w q_i(\xi_w, Q^2) + \xi_w \bar{q}_i(\xi_w, Q^2)]]
\end{aligned} \tag{47}$$

$$\begin{aligned}
2x\mathcal{F}_1^{\nu, cp}(x, Q^2) &= K_{charm} \\
&\times \frac{1 + 4M^2 x^2 / Q^2}{1 + R(\xi_w, Q^2)} \mathcal{F}_2^{cp}(x, Q^2)
\end{aligned} \tag{48}$$

and

$$\begin{aligned}
x\mathcal{F}_3^{\nu}(x, Q^2) &= 2H(x, Q^2)K_{charm} \\
&\left\{ \begin{aligned} &\Sigma_i K_i^{xF3} \xi_w q_i(\xi_w, Q^2) \\ &- \Sigma_j K_j^{xF3} \xi_w \bar{q}_j(\xi_w, Q^2) \end{aligned} \right\}
\end{aligned} \tag{49}$$

Here we use the  $R_{1998}$  parametrization [19] for the vector part of  $R^{ncp}$  and  $R^{cp}$

### 13. Nuclear corrections

In the comparison with neutrino charged-current differential cross section on iron, a nuclear correction for iron targets should be applied. Previously, we used the following parameterized function,  $f(x)$  (a fit to experimental electron and muon scattering data for the ratio of iron to deuterium cross sections, shown in Fig 11), to convert deuterium structure functions to (isoscalar) iron structure functions [45];

$$\begin{aligned}
f(x) &= 1.096 - 0.364 x - 0.278 e^{-21.94 x} \\
&+ 2.772 x^{14.417}
\end{aligned} \tag{50}$$

However, we find that the ratios of iron to deuterium structure functions from SLAC and Jefferson Lab are better described in terms of the variable  $\xi_w$ . In addition, if  $\xi_w$  is used, the function that describes the iron to deuterium ratios in the deep inelastic region is also valid in the

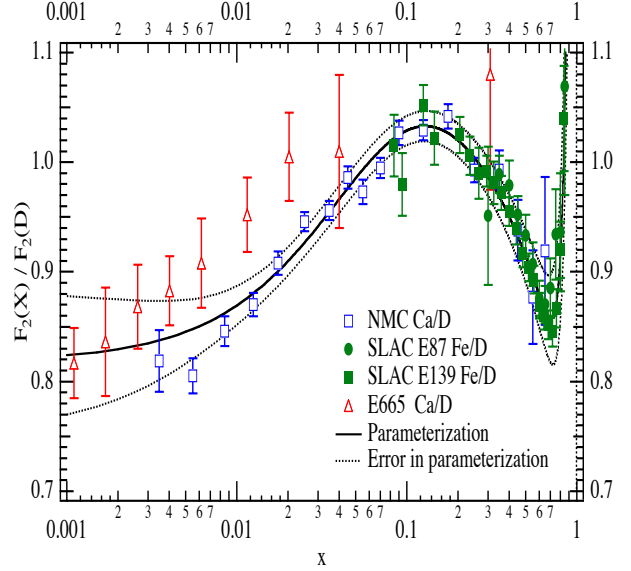


Figure 11. The ratio of  $\mathcal{F}_2$  data for heavy nuclear targets and deuterium as measured in charged lepton scattering experiments (SLAC, NMC, E665). The band shows the uncertainty of the parametrized curve from the statistical and systematic errors in the experimental data [45].

resonance region. Therefore, we use the following updated function  $\mathcal{F}_{updated}(\xi_w)$ .

$$\begin{aligned}
\mathcal{F}_{updated}(\xi_w) &= 1.096 - 0.364 \xi_w \\
&- 0.278 e^{-21.94 \xi_w} + 8 \xi_w^{14.417}
\end{aligned} \tag{51}$$

Figure 12 shows a comparison of Jefferson lab measurements of ratio of the cross sections on iron to deuterium in the resonance region [46] to data from SLAC E87 and SLAC E139 in the deep inelastic region. The data are plotted versus  $x$  and are compared to the fit function  $f(x)$ . Figure 13 shows the same data plotted versus  $\xi_w$  and are compared to our updated fit function  $\mathcal{F}_{updated}(\xi_w)$ . When plotted versus  $\xi_w$  the ratios in the deep inelastic region and the ratios in the resonance region all lie on the same universal curve.

For the ratio of deuterium cross sections to



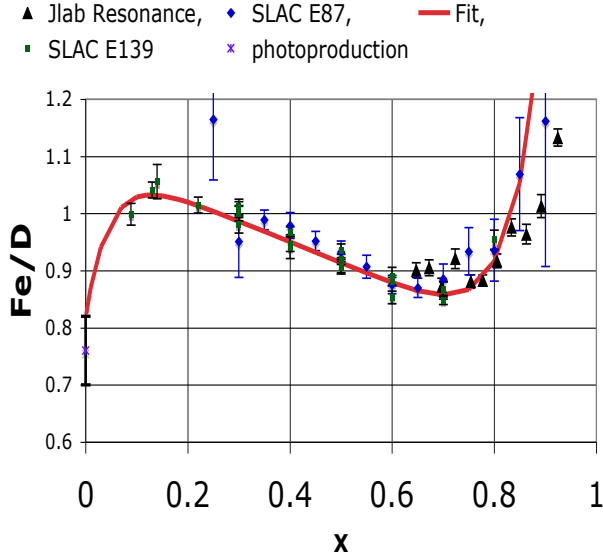


Figure 12. The ratio of  $\mathcal{F}_2$  data for heavy nuclear targets and deuterium as measured in charged lepton scattering experiments in the deep inelastic region (SLAC E87 and SLAC E139) as compared to Jlab data in the resonance region. The scatter of the points when plotted versus  $x$  is large. This illustrates that the ratio does not scale well with the variable  $x$ . Also shown is  $f(x)$ , which is a fit to all charged lepton scattering data as a function of  $x$

cross sections on free nucleons we use the following function obtained from a fit to SLAC data on the nuclear dependence of electron scattering cross sections [18].

$$f(x) = 0.985 \times (1 + 0.422x - 2.745x^2 + 7.570x^3 - 10.335x^4 + 5.422x^5). \quad (52)$$

This correction shown in Fig. 14 is only valid in the  $0.05 < x < 0.75$  region.

In neutrino scattering, we assume that the nuclear correction factor for  $\mathcal{F}_2$ ,  $x\mathcal{F}_3$  and  $2x\mathcal{F}_1$  are the same. This is a source of systematic error because the nuclear shadowing corrections at low  $x$  can be different for the vector and axial structure functions. This difference can be accounted for

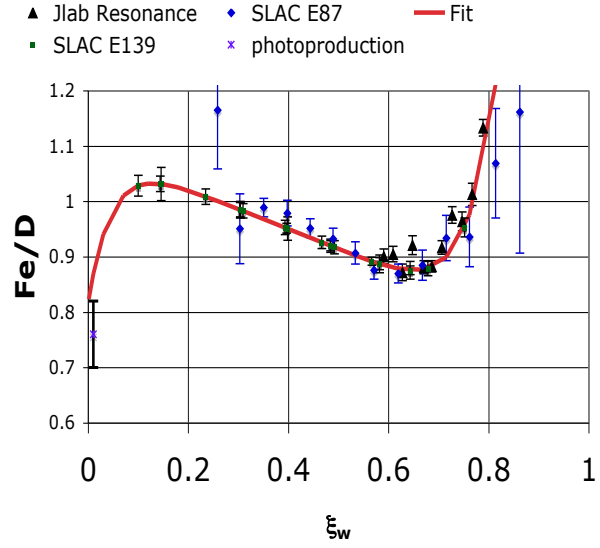


Figure 13. The ratio of  $\mathcal{F}_2$  data for heavy nuclear targets and deuterium as measured in charged lepton scattering experiments in the deep inelastic region (SLAC E87 and SLAC E139) as compared to Jlab data in the resonance region as a function of  $\xi_w$ . The scatter of the points when plotted versus  $\xi_w$  is smaller than when plotted versus  $x$ . This illustrates that the ratio scales better in the variable  $\xi_w$ . Also shown is  $\mathcal{F}_{updated}(\xi_w)$ , which is a revised fit to charged lepton scattering data as a function of  $\xi_w$ .

by assuming a specific theoretical model[40].

#### 14. d/u correction

The  $d/u$  correction for the GRV98 LO PDFs is obtained from the NMC data for  $\mathcal{F}_2^D/\mathcal{F}_2^P$ . Here, Eq. 52 is used to remove nuclear binding effects in the NMC deuterium  $\mathcal{F}_2$  data. The correction term,  $\delta(d/u)$  is obtained by keeping the total valence and sea quarks the same.

$$\delta(d/u)(x) = -0.00817 + 0.0506x + 0.0798x^2, \quad (53)$$

where the corrected  $d/u$  ratio is  $(d/u)' = (d/u) + \delta(d/u)$ . Thus, the modified  $u$  and  $d$  valence dis-

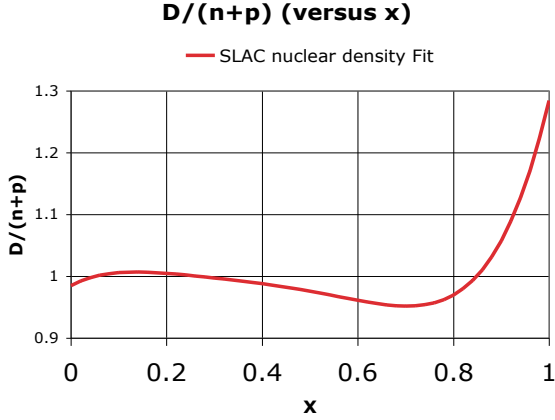


Figure 14. The total correction for nuclear effects (binding and Fermi motion) in the deuteron,  $\mathcal{F}_2^d/\mathcal{F}_2^{n+p}$ , as a function of  $x$ , extracted from fits to the nuclear dependence of SLAC  $\mathcal{F}_2$  electron scattering data. This correction is only valid in the  $0.05 < x < 0.75$  region.

tributions are given by

$$u'_v = \frac{u_v}{1 + \delta(d/u) \frac{u_v}{u_v + d_v}} \quad (54)$$

$$d'_v = \frac{d_v + u_v \delta(d/u) \frac{u_v}{u_v + d_v}}{1 + \delta(d/u) \frac{u_v}{u_v + d_v}}. \quad (55)$$

The same formalism is applied to the modified  $u$  and  $d$  sea distributions. Accidentaly, the modified  $u$  and  $d$  sea distributions (based on NMC data) agree with the NUSEA data in the range of  $x$  between 0.1 and 0.4. Thus, we find that corrections to  $u$  and  $d$  sea distributions are not necessary.

## 15. The Adler sum rule

The Adler sum rules are derived from current algebra and are therefore valid at all values of  $Q^2$ . The equations below are only for the *strangeness conserving*(*sc*) part of the structure functions. These are related to the PDFs by a factor of  $\cos^2\theta_c$ .

The Adler sum rules for the vector part of the

structure function  $\mathcal{W}_2^{\nu-vector}$  is given by:

$$|F_V^1(Q^2)|^2 + \int_{\nu_0}^{\infty} \mathcal{W}_{2n-sc}^{\nu-vector}(\nu, Q^2) d\nu - \int_{\nu_0}^{\infty} \mathcal{W}_{2p-sc}^{\nu-vector}(\nu, Q^2) d\nu = 1 \quad (56)$$

Where the limits of the integrals are from pion threshold  $\nu_0$  where  $W = M_\pi + M_P$  to  $\nu = \infty$ . At  $Q^2 = 0$ , the inelastic part of  $\mathcal{W}_2^{\nu-vector}$  goes to zero, and the sum rule is saturated by the quasielastic contribution  $|F_V^1(Q^2)|^2$ . Here  $\tau = Q^2/4M^2$ , and

$$F_V^1(Q^2) = \frac{G_E^V(Q^2) + \tau G_M^V(Q^2)}{1 + \tau},$$

In the dipole approximation (discussed in an Appendix) we have

$$G_E^V(Q^2) = G_D(Q^2)$$

$$G_M^V(Q^2) = 4.706 G_D(Q^2)$$

$$G_D = 1/(1 + Q^2/M_V^2)^2$$

Where  $M_V^2 = 0.71 (GeV/c)^2$

The Adler sum rule for  $\mathcal{W}_2^{\nu-axial}$  is given by:

$$|\mathcal{F}_A(Q^2)|^2 + \int_{\nu_0}^{\infty} \mathcal{W}_{2n-sc}^{\nu-axial}(\nu, Q^2) d\nu - \int_{\nu_0}^{\infty} \mathcal{W}_{2p-sc}^{\nu-axial}(\nu, Q^2) d\nu = 1$$

where in the dipole approximation

$$\mathcal{F}_A = -1.267/(1 + Q^2/M_A^2)^2$$

and  $M_A = 1.014 GeV/c^2$  from reference[52].

The Adler sum rule for  $\mathcal{W}_1^{\nu-vector}$  is given by:

$$\tau |G_M^V(Q^2)|^2 + \int_{\nu_0}^{\infty} \mathcal{W}_{1n}^{\nu-vector}(\nu, Q^2) d\nu - \int_{\nu_0}^{\infty} \mathcal{W}_{1p}^{\nu-vector}(\nu, Q^2) d\nu = 1 \quad (57)$$

The Adler sum rule for  $\mathcal{W}_1^{\nu-axial}$  is given by:

$$(1 + \tau) |\mathcal{F}_A(Q^2)|^2 + \int_{\nu_0}^{\infty} \mathcal{W}_{1n-sc}^{\nu-axial}(\nu, Q^2) d\nu - \int_{\nu_0}^{\infty} \mathcal{W}_{1p-sc}^{\nu-axial}(\nu, Q^2) d\nu = 1 \quad (58)$$

The Adler sum rule for  $\mathcal{W}_3^\nu$  is given by:

$$2\mathcal{F}_A(Q^2)G_M^V(Q^2) + \int_{\nu_0}^{\infty} \mathcal{W}_{3n-sc}^\nu(\nu, Q^2)d\nu - \int_{\nu_0}^{\infty} \mathcal{W}_{3p-sc}^\nu(\nu, Q^2)d\nu = 0 \quad (59)$$

### 16. Using the Adler sum rule to constrain the parameters of the model

We use the Adler sum rule for  $\mathcal{W}_2^{\nu-vector}$  to constrain the form of the  $K_{valence}^{vector}(Q^2)$  factor for  $\mathcal{W}_2^{\nu-vector}$ . At low  $Q^2$  we approximate

$$\frac{(G_E^V)^2(Q^2) + \tau(G_M^V(Q^2))^2}{(1 + \tau)}$$

by  $G_D^2(Q^2)$ , and use the following  $K$  factors for  $\mathcal{W}_2^{\nu-vector}$ .

$$K_{valence}^{vector}(Q^2) = [1 - G_D^2(Q^2)] \times \left( \frac{Q^2 + C_{v2}}{Q^2 + C_{v1}} \right) \quad (60)$$

where the additional parameters are obtained from a fit to the data. With this  $K_{valence}^{vector}(Q^2)$  factor, the Adler sum rule for  $\mathcal{W}_2^{\nu-vector}$  is then approximately satisfied. At  $Q^2 = 0$ , the inelastic part of  $\mathcal{W}_2^{\nu-vector}$  goes to zero, and the sum rule is saturated by the quasielastic contribution.

In the limit of  $Q^2 = 0$  the Adler sum rules for  $\mathcal{W}_2^{axial}$  and  $\mathcal{W}_1^{axial}$  are the same. Therefore, we make the assumption that:

$$\mathcal{W}_1^{axial}(\nu, Q^2 = 0) = \mathcal{W}_2^{axial}(\nu, Q^2 = 0)$$

Our model is supposed to be used to estimate the cross section for  $W > 1.9 \text{ GeV}/c^2$ . For  $W < 1.9 \text{ GeV}/c^2$ , it is best to use a detailed resonance production model[34,35], which should also includes a non-resonant background. However, since our model is constructed to provide a reasonable average of the cross section in the resonance region (above pion threshold,  $W = 1.1 \text{ GeV}/c^2$ ), the transition between a resonance production model and our model should be smooth. Note that in addition, the quasielastic contribution needs to be added separately.

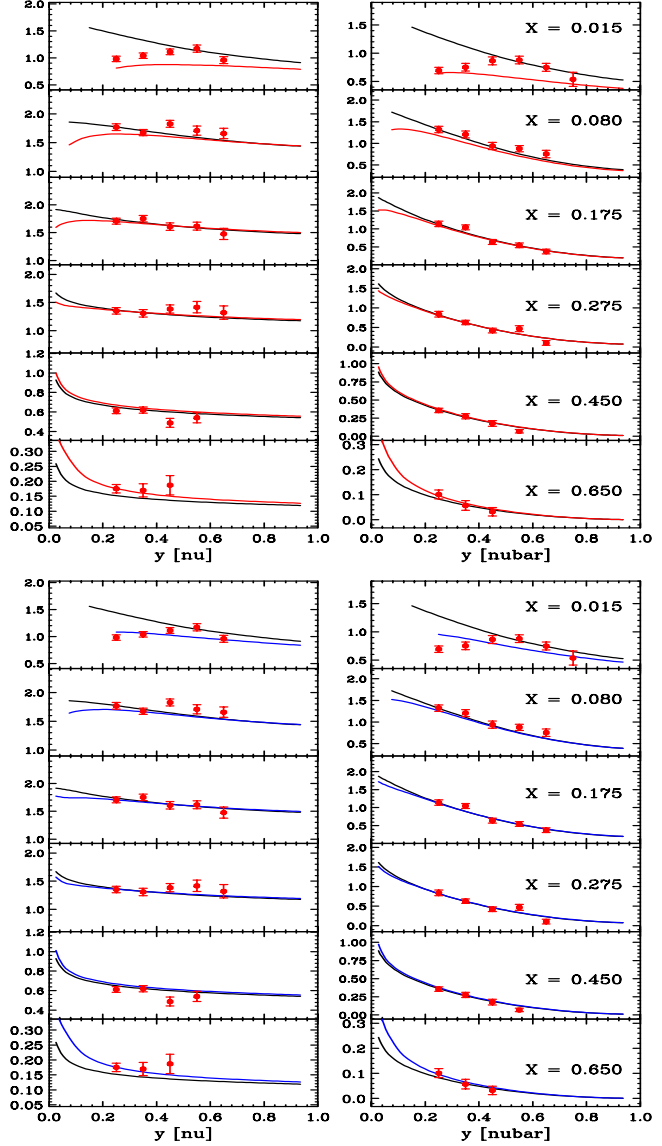


Figure 15. CCFR differential cross sections  $d^2\sigma/dx dy$  on iron (in units of  $10^{-38} \text{ cm}^2$ ) for neutrinos (left) and antineutrinos (right) at an energy of 55 GeV. The black lines in both (top and bottom) figures uses the default GRV98 PDFs without our modifications, The red line on the top figure is the lower limit of our predictions ( $K_{axial} = K_{vector}$ ), and the blue line in the bottom figure is our prediction with the suggested axial  $K$  factors.

## 17. Comparison to Neutrino Data on Heavy Targets

Figure 15 shows comparisons of the model to charged-current neutrino and antineutrino differential cross section data on iron from CCFR [18, 47] at an energy of 55  $GeV$ . On the left side we show the comparison for neutrino cross sections and on the right side we show the prediction for antineutrinos. In top figure the black curve is the prediction from GRV98 PDFs without our modifications, and the red line is the prediction from our model under the assumption that the axial  $K$  factors are the same as the vector  $K$  factors. We consider this case to be a lower limit on the error band of our prediction. In the bottom figure, the black curve is the also prediction from GRV98 PDFs without our modifications, and the blue line is the prediction from our model with our suggested axial  $K$  factors.

Figure 16 shows the same comparisons of our model to charged-current neutrino and antineutrino differential cross section data on iron from CCFR [18,47] at an energy of 35  $GeV$ . The CCFR data are corrected for radiative correction. Therefore, no radiative corrections are applied to the model predictions. However, the data are not corrected for non-isoscalar target (neutron excess). Therefore, our prediction are calculated for a non-isoscalar target. In both Figure 15 and Figure 16 we applied the nuclear corrections from our fits to charged lepton scattering data to the model.

We assume that the nuclear correction factor for  $\mathcal{F}_2$ ,  $x\mathcal{F}_3$  and  $2x\mathcal{F}_1$ . This is a source of systematic error because the nuclear shadowing corrections at low  $x$  can be different for the vector and axial structure functions. This difference can be accounted for by assuming a specific theoretical model[40].

We find that our predictions are in good agreement with the CCFR [18,47] data. neutrino and antineutrino differential cross sections, except for a small difference at the lowest values of  $x$ . This is the region which is most sensitive to the axial  $K$  factors for the sea quarks, and nuclear shadowing (which may in general be different neutrino and charged lepton scattering).

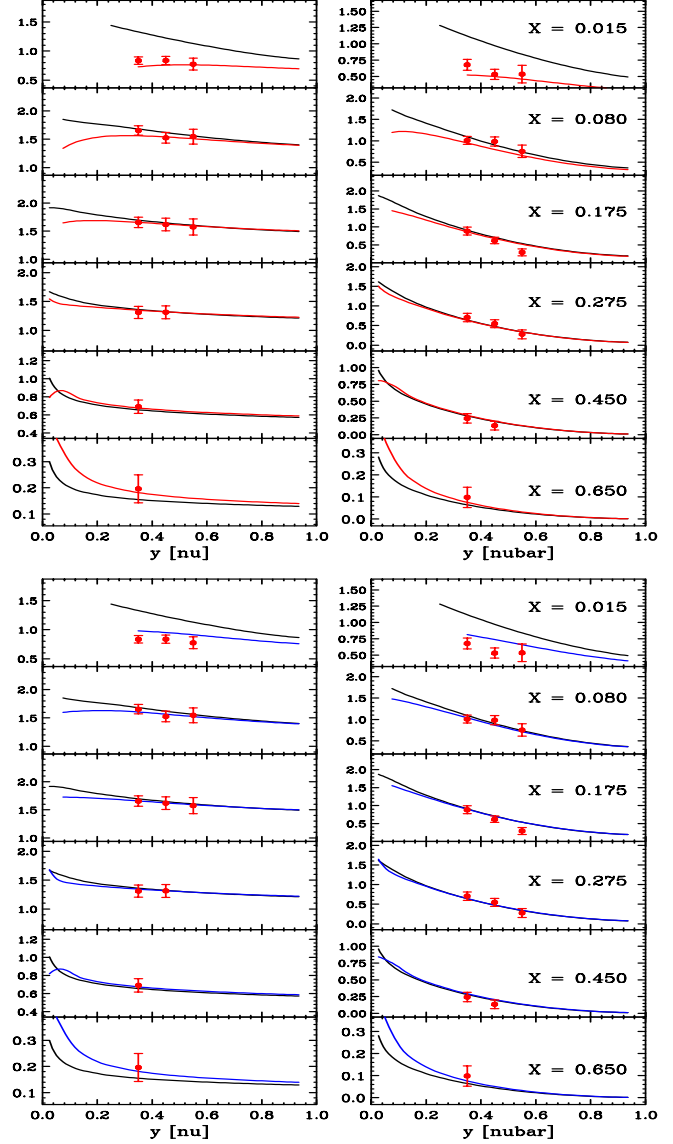


Figure 16. CCFR differential cross sections  $d^2\sigma/dx dy$  on iron (in units of  $10^{-38} \text{ cm}^2$ ) for neutrinos (left) and antineutrinos (right) at an energy of 35  $GeV$ . The black lines in both (top and bottom) figures uses the default GRV98 PDFs without our modifications, The red line on the top figure is the lower limit of our predictions ( $K_{axial} = K_{vector}$ ), and the blue line in the bottom figure is our prediction with the suggested axial  $K$  factors.

Note however, that the lowest  $x$  region does not contribute much to low energy neutrino cross sections Monte Carlo where our model has been primarily used [13,14,15]. Therefore, we plan to use include neutrino data at low energies from the MINERvA [9] experiment when these data becomes available in the future.

The data are also consistent with measurements from CDHSW [48] and CHORUS [49]. Figures 17, 18, 19, 20, and 21 show comparisons of our model to charged-current neutrino and antineutrino differential cross section data from CHORUS [49] at energies of 15, 25, 35, 45, 55, 70, 90, 110 and 130  $GeV$ . The CHORUS data are on a lead target, The CHORUS data are corrected for radiative correction and non-isoscalar target (using the correction values provided in the CHORUS publication). However, the data are not corrected for nuclear corrections for the lead target. In the comparison, our prediction are for for an iron target. Therefore, some small differences between our predictions and the CHORUS data are expected because of differences in the nuclear corrections between iron and lead.

## 18. Systematic errors in the application of the model

The model represents all charged lepton scattering data in the deep inelastic region ( $W > 1.9 GeV/c^2$ ) on hydrogen and deuterium down to  $Q^2 = 0$ . Therefore, under the assumption of CVC, the vector part of the cross section in neutrino scattering is modeled at the 5% level. Therefore, the systematic error in the model prediction is dominated by other sources as described below.

- Radiative corrections: The model predicts neutrino cross sections at the Born level. Therefore, radiative corrections must be applied to the model if it is compared to non-radiatively corrected neutrino or charged lepton data.
- Charm sea: Since the GRBV98 PDFs do not include a charm sea, the charm sea contribution must be added separately. This can be implemented either by using

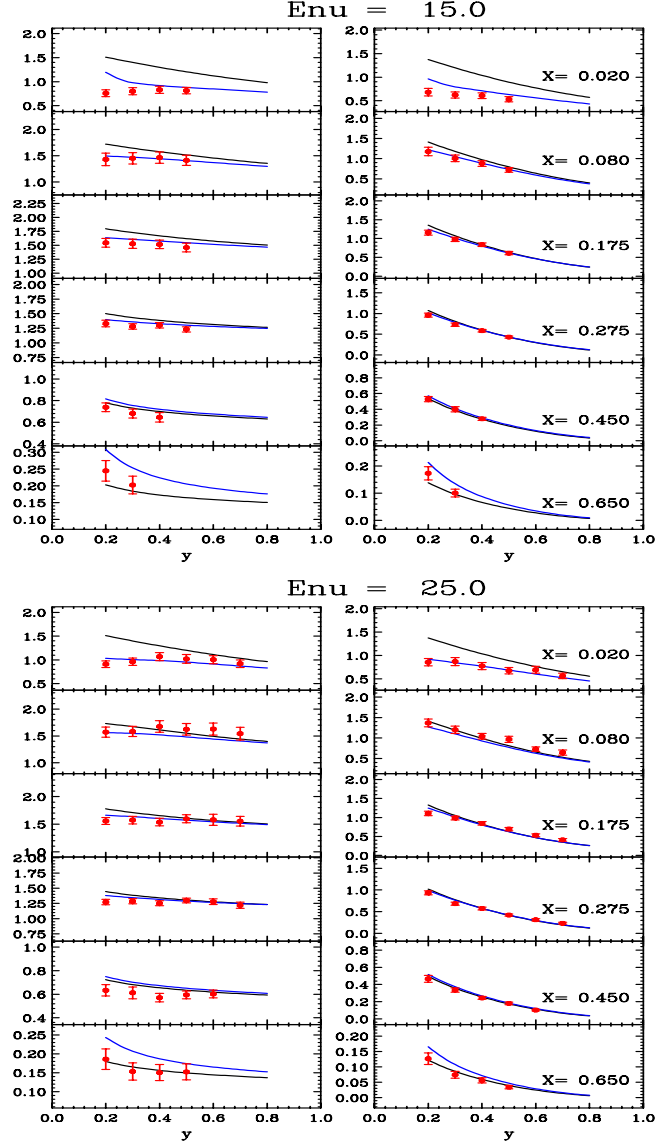


Figure 17. CHORUS differential cross sections  $d^2\sigma/dx dy$  on lead (in units of  $10^{-38} cm^2$ ) for neutrinos (left) and antineutrinos (right) at energies of 15 and 25  $GeV$ . The black lines in both (top and bottom) figures uses the default GRV98 PDFs without our modifications, the blue line in the bottom figure is our prediction with the suggested axial  $K$  factors (using nuclear corrections for iron).

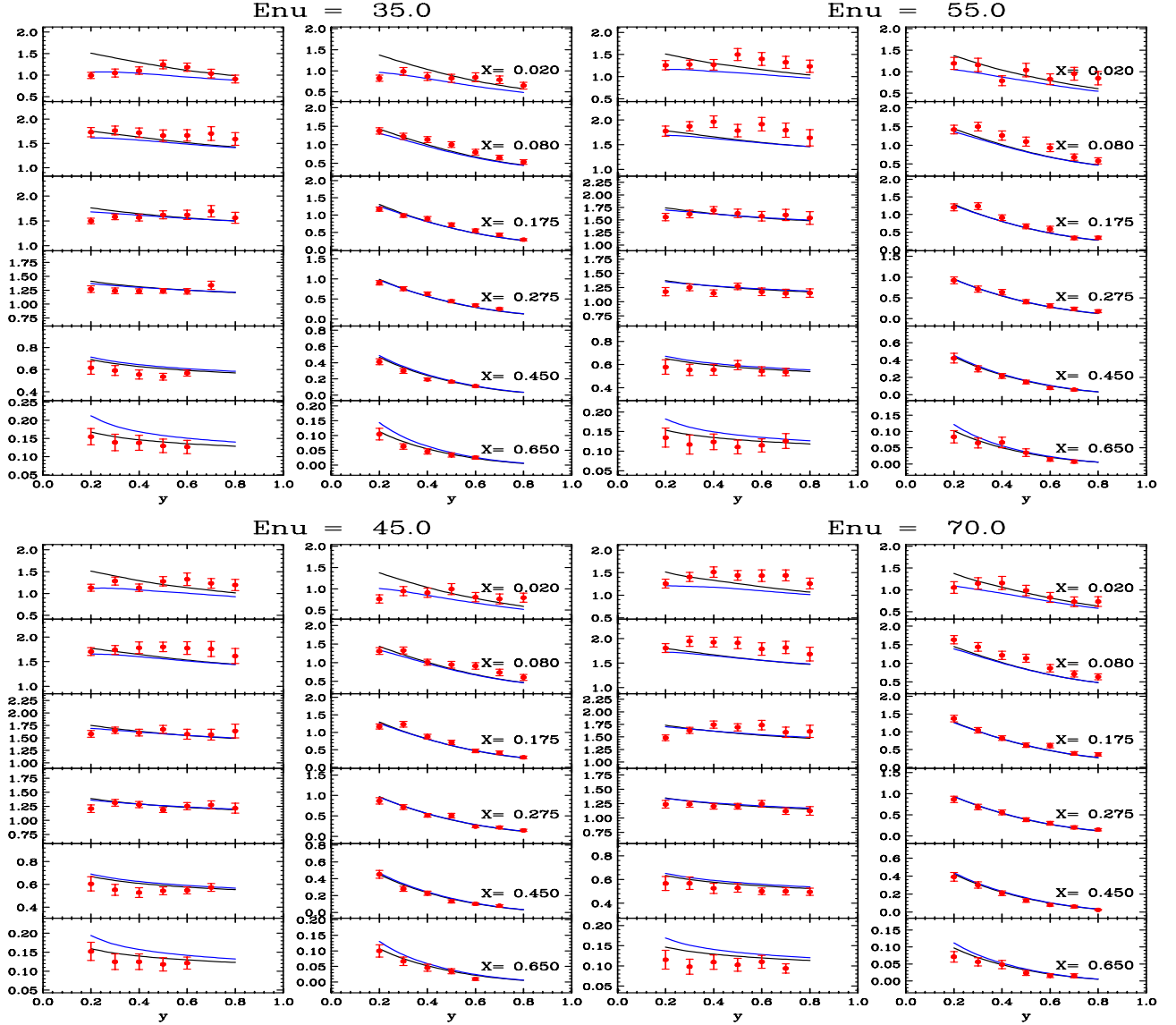


Figure 18. CHORUS differential cross sections  $d^2\sigma/dx dy$  on lead (in units of  $10^{-38} \text{ cm}^2$ ) for neutrinos (left) and antineutrinos (right) at energies of 35 and 45 GeV. The black lines in both (top and bottom) figures uses the default GRV98 PDFs without our modifications, the blue line in the bottom figure is our prediction with the suggested axial  $K$  factors (using nuclear corrections for iron).

Figure 19. CHORUS differential cross sections  $d^2\sigma/dx dy$  on lead (in units of  $10^{-38} \text{ cm}^2$ ) for neutrinos (left) and antineutrinos (right) at energies of 55 and 70 GeV. The black lines in both (top and bottom) figures uses the default GRV98 PDFs without our modifications, the blue line in the bottom figure is our prediction with the suggested axial  $K$  factors (using nuclear corrections for iron).

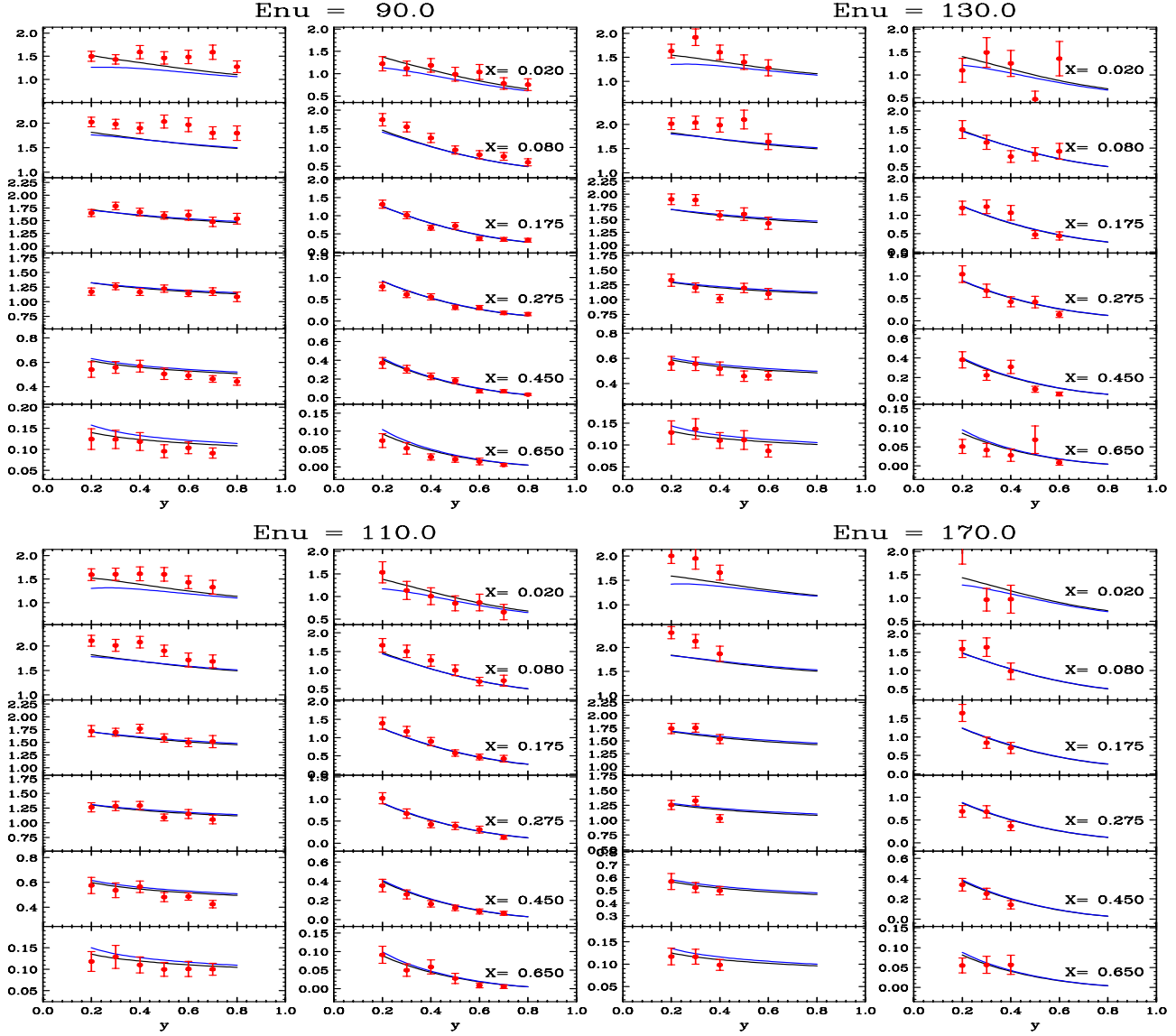


Figure 20. CHORUS differential cross sections  $d^2\sigma/dxdy$  on lead (in units of  $10^{-38} \text{ cm}^2$ ) for neutrinos (left) and antineutrinos (right) at energies of 90 and 110 GeV. The black lines in both (top and bottom) figures uses the default GRV98 PDFs without our modifications, the blue line in the bottom figure is our prediction with the suggested axial  $K$  factors (using nuclear corrections for iron).

Figure 21. CHORUS differential cross sections  $d^2\sigma/dxdy$  on lead (in units of  $10^{-38} \text{ cm}^2$ ) for neutrinos (left) and antineutrinos (right) at energies of 90 and 110 GeV. The black lines in both (top and bottom) figures uses the default GRV98 PDFs without our modifications, the blue line in the bottom figure is our prediction with the suggested axial  $K$  factors (using nuclear corrections for iron).



a boson-gluon fusion model, or by incorporating a charm sea from another set of PDFs. Therefore, unless the charm sea contribution is added, the model will underestimate the cross section at high neutrino energies and large values of  $\nu$ . We modeled the contribution of the charm sea using a photon-gluon fusion model when we compared our predictions to photoproduction data at HERA. Note that at low neutrino energies the charm sea correction is very small.

- Axial  $K$  factors for sea quarks: We assume  $P = 0.6 \pm 0.3$ . With this assumption, the suggested axial  $K$  factors for the up, down and strange sea quarks and antiquarks lie between the assumption that the axial  $K$  factors for the sea are the same as the vector  $K$  factors for the sea (which yields a lower limit) and the assumption that the axial  $K$  factors for the sea are equal to 1 (which yields an upper limit). These lower and upper limits can be taken as an estimate of the systematic error originating from this source.
- Axial  $K$  factors for valence quarks: For the sea quarks, the vector  $K$  factor is approximately 0.5 at  $Q^2 = 0.4 \text{ (GeV/c)}^2$ . For valence quarks, the vector  $K$  factor is approximately 0.5 at a lower value of  $Q^2 = 0.18 \text{ (GeV/c)}^2$ . We have made the assumption that the axial  $K$  factors for valence quarks is equal to 1. This assumption gives the correct neutron-proton average cross section for the  $\Delta(1232)$  resonance at  $Q^2 = 0$ . Here again, taking half of the difference between assuming that the valence axial  $K$  factor is equal to 1, and the assumption that the valence axial  $K$  factor is the same as the valence vector  $K$  factor can be taken as the systematic error from this source.
- Nuclear corrections: We have assumed that the nuclear corrections for the axial and vector case are the same, and equal to the nuclear corrections measured in charged

lepton scattering. We have also assumed that they are the same for all three structure functions, and that these corrections can be applied by using a simple fit in  $x_w$ . The systematic error from this source can be reduced by using specific theoretical models[40] to account for the differences in the nuclear corrections between neutrino and charged lepton scattering as a function of  $Q^2$  and  $x$  for various nuclear targets. Because of the uncertainty in the nuclear corrections, we chose to model neutrino and charged lepton scattering on hydrogen and deuterium only, and we did not include any neutrino data (which are mostly on nuclear targets) in our fits at this stage.

- A better determination of the axial  $K$  factors for the sea quarks requires including neutrino data (e.g. CCFR, CDHS, CHORUS, NOMAD and MINERvA) on nuclear targets in our fit. The nuclear corrections at small  $x$  for vector and axial structure functions are different in general. Therefore, it is not possible to separately determining the axial  $K$  factor without assuming a specific model for the neutrino nuclear corrections[40]. This study will be presented in a future communication.

## 19. Using the model near $Q^2 = 0$

Near  $Q^2 = 0$  and  $x = 0$  there are terms in the expression for the cross section that are proportional to the square of the muon mass as shown in equation 35. In the low  $Q^2$  region it is more convenient to use the structure functions  $\mathcal{F}_1 = M\mathcal{W}_1$ ,  $\mathcal{F}_2 = \nu\mathcal{W}_2$ , and  $\mathcal{F}_3 = \nu\mathcal{W}_3$ , instead of  $2x\mathcal{F}_1$  and  $x\mathcal{F}_3$  which are more useful at higher  $Q^2$ .

The expression for the scaling variable  $\xi_w$

$$\xi_w = \frac{2x(Q^2 + M_f^2 + B)}{Q^2[1 + \sqrt{1 + 4M^2x^2/Q^2}] + 2Ax}, \quad (61)$$

can be written alternatively as

$$\xi_w = \frac{(Q^2 + M_f^2 + B)}{M\nu[1 + \sqrt{1 + Q^2/\nu^2}] + A}, \quad (62)$$



The structure function  $2x\mathcal{F}_1$  should be divided by  $2x$  to yield  $\mathcal{F}_1$  and the structure function  $x\mathcal{F}_3$  should be divided by  $x$  to get  $\mathcal{F}_3$ . Note the  $\mathcal{F}_1$  and  $\mathcal{F}_3$  (or alternatively  $\mathcal{W}_1$  and  $\mathcal{W}_3$ ) structure functions do not diverge at  $Q^2 = 0$ . This because  $2x\mathcal{F}_1$  and  $x\mathcal{F}_3$  are proportional to  $Q^2$  near  $Q^2 = 0$  (because of the various  $K$  factors).

For example, the valence  $d$  quark component of  $\mathcal{F}_3$  is given by:

$$\mathcal{F}_3^{valence-down}(Q^2, W) = \frac{2}{x} \sqrt{\frac{Q^2[1-G_D^2(Q^2)]}{Q^2+C_{xF3}}} \\ \times K_{\nu d}^{LW} \xi_w d_{valence}(\xi_w, Q^2) \left( \frac{Q^2+C_{v2d}^{vector}}{Q^2+C_{v1d}^{vector}} \right)$$

At low  $Q^2$  the vector  $K$  factor for valence quarks  $[1-G_D^2(Q^2)]$  can be written as  $Q^2/(Q^2+0.178)$ , which yields.

$$\mathcal{F}_3^{valence-down}(Q^2, W) = \frac{2M\nu}{\sqrt{(Q^2+C_{xF3})(Q^2+0.178)}} \\ \times K_{\nu d}^{LW} \xi_w u_{valence}(\xi_w, Q^2) \left( \frac{Q^2+C_{v2d}^{vector}}{Q^2+C_{v1d}^{vector}} \right)$$

## 20. Using the model to determine the flux of low energy neutrino beams

It is very difficult to make a good measurement of the neutrino and antineutrino flux as a function of energy in a broad band beam such as the NUMI beam. The following technique can be used to extract the flux directly from the data.

The model gives a very good prediction of the neutrino differential cross sections in a restricted region of phase space. This region corresponds to  $W > 1.9 \text{ GeV}/c^2$  (the inelastic region)  $Q^2 > 1 \text{ (GeV}/c)^2$  (where vector and axial structure functions are close to each other) and  $x > 0.1$  (where nuclear effects in neutrino and charged lepton scattering should be very similar). The data in this restricted region can be used to determine the neutrino and antineutrino flux by comparing it to our model predictions.

At very low energies there may not be many events in the region of validity of our model. However, we can cross calibrate between high and low energies by using events at a fixed range of  $W$  and  $Q^2 < 1 \text{ (GeV}/c)^2$ . This is because as can be inferred from equation 35, the differential cross section for

a fixed range of  $W$  and low  $Q^2$  is dominated by  $\mathcal{W}_2$  and is relatively independent of neutrino energy, and the small energy dependent corrections given in equation 35 can be calculated. We will present a study of these two techniques in a future communication.

## 21. Appendix - Quasi-elastic Neutrino-Nucleon Scattering

In order to calculate the total neutrino and antineutrino total cross sections, we need to add the quasi-elastic cross sections. Here we use the notation of C.H. Llewellyn Smith [51]

$$q^2 = q_0^2 - \vec{q}_3^2 = -4E_0 E' \sin^2 \frac{\theta}{2} = -Q^2.$$

The hadronic current for QE neutrino scattering is given by [51]

$$< p(p_2) | J_\lambda^+ | n(p_1) > = \\ \bar{u}(p_2) \left[ \gamma_\lambda \mathcal{F}_V^1(q^2) + \frac{i\sigma_{\lambda\nu} q^\nu \xi \mathcal{F}_V^2(q^2)}{2M} \right. \\ \left. + \gamma_\lambda \gamma_5 \mathcal{F}_A(q^2) + \frac{q_\lambda \gamma_5 \mathcal{F}_P(q^2)}{M} \right] u(p_1),$$

where  $q = k_\nu - k_\mu$ ,  $\xi = (\mu_p - 1) - \mu_n$ , and  $M = (m_p + m_n)/2$ . Here,  $\mu_p$  and  $\mu_n$  are the proton and neutron magnetic moments. We assume that there are no second class currents, so the scalar form factor  $\mathcal{F}_V^3$  and the tensor form factor  $\mathcal{F}_A^3$  need not be included. Using the above current, the cross section is

$$\frac{d\sigma^{\nu, \bar{\nu}}}{dq^2} = \frac{M^2 G_F^2 \cos^2 \theta_c}{8\pi E_\nu^2} \times \\ \left[ A(q^2) \mp \frac{(s-u)B(q^2)}{M^2} + \frac{C(q^2)(s-u)^2}{M^4} \right],$$

where

$$A(q^2) = \frac{m^2 - q^2}{4M^2} \left[ \left( 4 - \frac{q^2}{M^2} \right) |\mathcal{F}_A|^2 \right. \\ \left. - \left( 4 + \frac{q^2}{M^2} \right) |\mathcal{F}_V^1|^2 - \frac{q^2}{M^2} |\xi \mathcal{F}_V^2|^2 \left( 1 + \frac{q^2}{4M^2} \right) \right. \\ \left. - \frac{4q^2 \text{Re} \mathcal{F}_V^{1*} \xi \mathcal{F}_V^2}{M^2} \right],$$

$$B(q^2) = -\frac{q^2}{M^2} \text{Re} \mathcal{F}_A^* (\mathcal{F}_V^1 + \xi \mathcal{F}_V^2),$$

$$C(q^2) = \frac{1}{4} \left( |\mathcal{F}_A|^2 + |\mathcal{F}_V^1|^2 - \frac{q^2}{M^2} \left| \frac{\xi \mathcal{F}_V^2}{2} \right|^2 \right).$$

Although we have not shown terms of order  $(m_l/M)^2$ , and terms including  $\mathcal{F}_P(q^2)$  (which is multiplied by  $(m_l/M)^2$ ), these terms are included in our calculations [51].) The form factors  $F_V^1(q^2)$  and  $\xi F_V^2(q^2)$  are given by:

$$F_V^1(q^2) = \frac{G_E^V(q^2) - \frac{q^2}{4M^2} G_M^V(q^2)}{1 - \frac{q^2}{4M^2}},$$

$$\xi F_V^2(q^2) = \frac{G_M^V(q^2) - G_E^V(q^2)}{1 - \frac{q^2}{4M^2}}.$$

From conserved vector current (CVC)  $G_E^V(q^2)$  and  $G_M^V(q^2)$  are related to the electron scattering form factors  $G_E^p(q^2)$ ,  $G_E^n(q^2)$ ,  $G_M^p(q^2)$ , and  $G_M^n(q^2)$ :

$$G_E^V(q^2) = G_E^p(q^2) - G_E^n(q^2),$$

$$G_M^V(q^2) = G_M^p(q^2) - G_M^n(q^2).$$

At low  $Q^2$  the axial form factor  $\mathcal{F}_A$  can be approximated by the dipole form

$$\mathcal{F}_A(q^2) = \frac{g_A}{\left(1 - \frac{q^2}{M_A^2}\right)^2},$$

In our analysis we apply BBBA2008 corrections[52] to the the dipole parametrization of the axial form factor as described in reference[52].

The pseudoscalar form factor  $\mathcal{F}_P$  is related to  $\mathcal{F}_A$  by PCAC and is given by:

$$\mathcal{F}_P(q^2) = \frac{2M^2 \mathcal{F}_A(q^2)}{M_\pi^2 - q^2}.$$

In the expression for the cross section,  $\mathcal{F}_P(q^2)$  is multiplied by  $(m_l/M)^2$ . Therefore, in muon neutrino interactions, this effect is very small except at very low energy, below 0.2 GeV.

At low  $Q^2$  a reasonable description of the proton and neutron elastic form factors is given by the dipole approximation  $G_D = 1/(1+Q^2/0.71)^2$ .

The dipole approximation is a lowest-order attempt to incorporate the non-zero size of the proton into the form factors. If we also assume that the proton has a simple exponential spatial charge distribution:

$$\rho(r) = \rho_0 e^{-r/r_0} \quad (63)$$

where  $r_0$  is the scale of the proton radius. The form factors are related, in the non-relativistic limit, to the Fourier transform of the charge and magnetic moment distribution. If it is also assumed that the magnetic moment distribution has the same spatial dependence as the charge distribution (*i.e.*, form factor scaling), we get the dipole approximation to the form factors:

$$\begin{aligned} G_D(Q^2) &\equiv \frac{1}{(1 + Q^2 r_0^2)^2} \\ &\equiv \frac{1}{(1 + Q^2/0.71)^2} \\ &= G_E^p(Q^2) \\ &= G_M^p(Q^2)/\mu_p \\ &= G_M^n(Q^2)/\mu_n \end{aligned}$$

and  $G_E^n = 0$ . Here  $\mu_p = 2.7928$ , and  $\mu_n = 1.913$ . Previous measurements of  $e-p$  and  $e-n$  elastic scattering have indicated a best fit value of  $r_0^2 = (0.24 \text{ fm})^2 = 1/0.71 \text{ (GeV/c)}^2$ , indicating an rms radius of  $\sqrt{\langle r^2 \rangle} \approx 0.81 \text{ fm}$ . Measurements of  $G_E^p$  and  $G_M^p$  agree with the dipole approximation only for  $Q^2 < 1 \text{ (GeV/c)}^2$ . The dipole approximation yields.

$$G_M^V(Q^2) = 4.706 G_D(Q^2)$$

Using  $\tau = Q^2/M^2$  we also get

$$F_V^1(Q^2) = \frac{G_E^V(Q^2) + \tau G_M^V(Q^2)}{1 + \tau},$$

In our calculation of the quasi-elastic cross sections we apply BBBA2008 corrections to the dipole parametrization of the vector form factors [52].

In evaluating the quasielastic contributions to the Adler sum rules we use:

$$W_{1n-elastic}^{\nu-vector} = \delta(\nu - \frac{Q^2}{2M} \tau) G_M^V(Q^2)^2$$

$$W_{1n-elastic}^{\nu-axial} = \delta(\nu - \frac{Q^2}{2M})(1 + \tau)|\mathcal{F}_A(Q^2)|^2$$

$$W_{2n-elastic}^{\nu-vector} = 2\frac{M\tau}{\nu}\delta(\nu - \frac{Q^2}{2M})|F_V^1(Q^2)|^2$$

$$W_{2n-elastic}^{\nu-axial} = 2\frac{M\tau}{\nu}\delta(\nu - \frac{Q^2}{2M})|\mathcal{F}_A(Q^2)|^2$$

$$W_{3n-elastic}^{\nu} = 2\frac{M\tau}{\nu}\delta(\nu - \frac{Q^2}{2M})|2G_M^V(Q^2)\mathcal{F}_A(Q^2)|$$

## 22. Appendix -Results with GRV94 PDFs and $x_w$

For completeness we describe our earlier analysis [10,11] in which we used another modified scaling variable [26]  $x_w$  with GRV94 PDFs (instead of GRV98) and simplified  $K$  factors. In that analysis we modified the leading order GRV94 PDFs as follows:

1. We increased the  $d/u$  ratio at high  $x$  as described in appendix A [16].
2. Instead of the scaling variable  $x$  we used the scaling variable  $x_w = (Q^2 + B)/(2M\nu + A)$  (or  $=x(Q^2 + B)/(Q^2 + Ax)$ ). This modification was used in early fits to SLAC data [27]. The parameter  $A$  provides for an approximate way to include *both* target mass and higher twist effects at high  $x$ , and the parameter  $B$  allows the fit to be used all the way down to the photoproduction limit ( $Q^2=0$ ).
3. In addition as was done in earlier non-QCD based fits [24,25] to low energy data, we multiplied all PDFs by a factor  $K=Q^2 / (Q^2 + C)$ . This was done in order for the fits to describe low  $Q^2$  data in the photoproduction limit, where  $\mathcal{F}_2$  is related to the photoproduction cross section.
4. Finally, we froze the evolution of the GRV94 PDFs at a value of  $Q^2 = 0.24$  (for  $Q^2 < 0.24$ ), because GRV94 PDFs are only valid down to  $Q^2 = 0.23$  ( $GeV/c$ )<sup>2</sup>.

As was done for GRV98, in the GRV94 analysis, the measured structure functions were also corrected for the BCDMS systematic error shift [20]

and for the relative normalizations between the SLAC, BCDMS and NMC data [16,17]. The deuterium data were corrected for nuclear binding effects [16,17]. A simultaneous fit to both proton and deuteron SLAC, NMC and BCDMS data (with  $x > 0.07$  only) yields  $A=1.735$ ,  $B=0.624$  and  $C=0.188$  ( $GeV/c$ )<sup>2</sup> with GRV94 LO PDFs ( $\chi^2 = 1351/958$  DOF). Note that for  $x_w$  the parameter  $A$  accounts for *both* target mass and higher twist effects.

In our studies with GRV94 PDFs we used the earlier  $R_{world}$  fit [19] for  $R^{ncp}$  and  $R^{cp}$ .  $R_{world}$  is parameterized by:

$$R_{world}(x, Q^2 > 0.35) = \frac{0.0635}{\log(Q^2/0.04)}\theta(x, Q^2) + \frac{0.5747}{Q^2} - \frac{0.3534}{Q^4 + 0.09}, \quad (64)$$

where  $\theta = 1. + \frac{12Q^2}{Q^2+1.0} \times \frac{0.125^2}{0.125^2+x^2}$ . The  $R_{world}$  function provided a good description of the world's data for  $R$  at that time in the  $Q^2 > 0.35$  ( $GeV/c$ )<sup>2</sup> and  $x > 0.05$  region (where most of the  $R$  data are available). However, for electron and muon scattering and for the vector part of neutrino scattering the  $R_{world}$  function breaks down below  $Q^2 = 0.35$  ( $GeV/c$ )<sup>2</sup>. Therefore, we freeze the function at  $Q^2 = 0.35$  ( $GeV/c$ )<sup>2</sup>. For electron and muon scattering and for the vector part of  $\mathcal{F}_1$  we introduce a  $K$  factor for  $R$  in the  $Q^2 < 0.35$  ( $GeV/c$ )<sup>2</sup> region. The new function provides a smooth transition for the vector  $R$  (we use  $R_{vector}=R_{e/\mu}$ ) from  $Q^2 = 0.35$  ( $GeV/c$ )<sup>2</sup> down to  $Q^2 = 0$  by forcing  $R_{vector}$  to approach zero at  $Q^2 = 0$  as expected in the photoproduction limit (while keeping a  $1/Q^2$  behavior at large  $Q^2$  and matching to  $R_{world}$  at  $Q^2 = 0.35$  ( $GeV/c$ )<sup>2</sup>).

$$R_{vector}(x, Q^2 < 0.35) = 3.207 \times \frac{Q^2}{Q^4 + 1} \times R_{world}(x, Q^2 = 0.35).$$

## REFERENCES

1. S. Fukuda *et al.*, Phys. Rev. Lett. **85**, 3999 (2000); T. Toshito, hep-ex/0105023.

2. D.G. Michael *et al.*, (MINOS) Phys. Rev. Lett. **97**, 191801 (2006); P. Adamson *et al.*, (MINOS) Phys. Rev. D **81**, 072002 (2010). <http://www-numi.fnal.gov/Minos/>
3. <http://www-nova.fnal.gov/>
4. M. H. Ahn *et al.*, (K2K) Phys. Rev. D **74**, 072003 (2006); <http://neutrino.kek.jp/>
5. Y. Itow *et al.*, (T2K) arXiv:hep-ex/0106019; <http://www-nova.fnal.gov/>
6. Y. Ashie *et al.*, (T2K) Phys. Rev. D **71**, 112005 (2005); <http://www-nova.fnal.gov/>
7. A. A. Aguilar-Arevalo *et al.*, (MiniBooNE) Phys. Rev. Lett. **98**, 231801(2007)
8. Y. Nakjima *et al.*, (SciBoonE) arXiv:hep-ex/1011.213
9. <http://minerva.fnal.gov/>
10. A. Bodek and U.K. Yang (NUINT01), Nucl. Phys. Proc. Suppl. **112**, 70 (2002) (hep-ex/0203009);
11. A. Bodek and U. K. Yang, (NUINT02) hep-ex/0308007.
12. Y. Hayato, Nucl Phys. Proc. Suppl.. **112**, 171 (2002)
13. C.Andreopoulos (GENIE), Nucl. Instrum. Meth.A614, 87,2010.
14. H. Gallagher, (NEUGEN) Nucl. Phys. Proc. Suppl. **112** (2002)
15. D. Casper (NUANCE), Nucl. Phys. Proc. Suppl. **112**, 161 (2002); <http://nuint.ps.uci.edu/nuance/>
16. U. K. Yang and A. Bodek, Phys. Rev. Lett. **82**, 2467 (1999).
17. U. K. Yang and A. Bodek, Eur. Phys. J. C **13**, 241 (2000).
18. U. K. Yang, Ph.D. thesis, Univ. of Rochester, UR-1583 (2001). <http://hep.uchicago.edu/~ukyang/neutrino/thesis.ps>.
19. L. W. Whitlow *et al.* (SLAC-MIT), Phys. Lett. B **282**, 433 (1995);
20. A. C. Benvenuti *et al.* (BCDMS), Phys. Lett. B **237**, 592 (1990); M. Virchaux and A. Milsztajn, Phys. Lett. B **274**, 221 (1992).
21. M. Arneodo *et al.* (NMC), Nucl. Phys. B **483**, 3 (1997).
22. H. Georgi and H. D. Politzer, Phys. Rev. D **14**, 1829 (1976); R. Barbieri *et al.*, Phys. Lett. B **64**, 171 (1976), and Nucl. Phys. B **117**, 50 (1976); J. Pestieau and J. Urias, Phys.Rev.D **8**, 1552 (1973)
23. M. Gluck, E. Reya, A. Vogt, Eur. Phys. J C **5**, 461 (1998).
24. A. Donnachie and P. V. Landshoff, Z. Phys. C **61**, 139 (1994)
25. B. T. Fleming *et al.* (CCFR), Phys. Rev. Lett. **86**, 5430 (2001).
26. F. W. Brasse *et al.*, Nucl.Phys.B39:421,1972.
27. A. Bodek *et al.*, Phys. Rev. D **20**, 1471 (1979).
28. S. Stein *et al.*, Phys. Rev. D **12**, 1884 (1975); K. Gottfried, Phys. Rev. Lett. **18**, 1174 (1967).
29. S. Adler, Phys. Rev. **143**, 1144 (1966); F. Gillman, Phys. Rev. **167**, 1365 (1968).
30. O. Lalakulich, W. Melnitchouk, and E. A. Paschos, Phys. Rev. C **75**::015202 (2007),
31. C. Adloff *et al.* (H1), Eur Phys J C **30**, 32 (2003); <http://www-h1.desy.de/>
32. David O. Caldwell, et al Phys.Rev.Lett. **25**, 609,1970; T.A. Armstrong et al. Nucl.Phys.B41, 445,(1972); T.A. Armstrong et al. Nov 1971. Published in Phys.Rev.D5, 1640,(1972); David O. Caldwell et al. Phys.Rev.Lett.40, 1222, (1978); S. Chekanov et al. (ZEUS) Nucl.Phys. B627, 3 (2002); T. Ahmed et al. (H1) Phys.Lett.B299 374 (1993).
33. C. Keppel, Proc. of the Workshop on Exclusive Processes at High  $P_T$ , Newport News, VA, May (2002).
34. O. Lalakulich and E. A. Paschos, Phys. Rev. D **71**::074003 (2005), and Phys. Rev. D **74**:014009 (2006).
35. D. Rein and L. M. Sehgal, Annals Phys. **133** 79 (1981); and R. Belusevic and D. Rein, Phys. Rev. D **46**, 3747 (1992).
36. E. D. Bloom and F. J. Gilman, Phys. Rev. Lett. **25**, 1140 (1970).
37. Y. Liang *et al.* [Jefferson Lab Hall C E94-110 Collaboration], arXiv:nucl-ex/0410027.
38. K. Abe *et al.*, Phys. Lett. B **452**, 194 (1999)
39. R.S. Thorne and R.G. Roberts, Phys. Lett. B **421**, 303 (1998); Eur. Phys. J. C **19**, 339 (2001).
40. S. A. Kulagin and R. Pett, Phys. Rev. D **76**, 094023 (2007), *ibid* Nucl. Phys. A **765** (26),2006.
41. S. Kretzer and M. H. Reno, Phys. Rev. D **66**,

- 113007 (2002); Yu Seon Jeong, M.H. Reno, Phys. Rev. D **82** 033010, 2010.
42. P. Allen et al, Nucl. Phys. B176, 269(1980)
  43. D. Allasia et al, Nucl. Phys. B343, 285 (1990).
  44. V.V. Ammosov et al. (FNAL E180) JETP Lett.43 716,1986, Pisma Zh.Eksp.Teor.Fiz.43 554,1986.
  45. W. G. Seligman, Ph.D. thesis, (CCFR) Columbia Univ., Nevis reports 292 (1997).
  46. J. Arrington et al, Phys.Rev. C**73**, 035205 (2006).
  47. U. K. Yang *et al.*(CCFR), Phys. Rev. Lett. **87**, 251802 (2001).
  48. P. Berge *et al.* (CDHSW), Zeit. Phys. **C49**, 607 (1991).
  49. R. Oldeman, Proc. of 30th International Conference on High-Energy Physics (ICHEP 2000), Osaka, Japan, 2000.
  50. Q. Wu *et al.*(NOMAD), Phys. Lett. **B60**, 19 (2008).
  51. C. H. Llewellyn Smith, Phys. Rep. 3C (1972); E. A. Paschos, Electroweak Theory, Cambridge University Press (2007).
  52. A. Bodek, S. Avvakumov, R. Bradford, and H. Budd, Eur. Phys. J. C**53**, 349 (2008).